Успехи физ. мет. / Usp. Fiz. Met. 2000, т. 1, сс. 9—48
Оттиски доступны непосредственно от издателя
Фотокопирование разрешено только
в соответствии с лицензией

МЕХАНИЧЕСКИЕ, ТЕПЛОВЫЕ И КИНЕТИЧЕСКИЕ СВОЙСТВА

PACS numbers: 61.72.Bb, 61.72.Ff, 61.72.Lk, 62.20.Fe, 81.40.Lm

Anomalies in Deformation Behaviour of TiAl Intermetallic

B. A. Greenberg and M. A. Ivanov*

Institute of Physics of Metals, Ural Division, Russian Academy of Sciences,
18 Sophia Kovalevskaya Str., 620219 Ekaterinburg, Russia
**G. V. Kurdyumov Institute for Metal Physics, N.A.S. of the Ukraine,*
36 Academician Vernadsky Blvd., UA -03680 Kyyiv-142, Ukraine

An explanation was proposed for a nonmonotonic temperature dependence of the yield stress $\sigma_y(T)$ in TiAl having two extrema where $\sigma_y(T)$ changes its temperature behaviour. The comparison of $\sigma_y(T)$ curves for TiAl and typical curves for other materials (b.c.c. metals, semiconductors, Ni_3Al-type intermetallics) allowed reconstructing the shape of the potential relief for dislocations in TiAl. The shape of the relief reflects existence of two types of dislocation traps (shallow and deep ones) and two types of potential barriers: low and high barriers for the capture of dislocations in shallow and deep traps respectively. The deformation behaviour of TiAl was described over the whole temperature interval allowing for the capture of dislocations in traps and their release therefrom. Expressions determining extremums of $\sigma_y(T)$ were derived. Possible dependences of the work hardening rate $\theta(T)$ in the region of the anomalous trend $\sigma_y(T)$ were analysed. Conditions of the anomalous behaviour of $\theta(T)$ were ascertained. It was proposed that the shape of the potential relief of a dislocation changed in the effective range of a microcrack. The capture of dislocations in deep traps, which is stimulated by concentration of stresses near a microcrack, and the inhibited release of dislocations from the traps up to relatively high temperatures are viewed as a possible cause of TiAl brittleness. A model of the deformation behaviour of intermetallics after prestraining was proposed. This model enables one to describe two alternatives: observation or absence of the stress macrojump after prestraining.

Предложено объяснение немонотонной температурной зависимости предела текучести $\sigma_y(T)$ в TiAl, где имеются две экстремальные точки, в которых происходит смена характера температурной зависимости $\sigma_y(T)$. Сравнение кривых $\sigma_y(T)$ для TiAl и типичных кривых для других материалов (ОЦК металлов, интерметаллидов типа Ni_3Al) позволяет реконструировать форму потенциального рельефа для дислокаций в TiAl. Форма полученного рельефа отражает существование двух типов дислокационных ловушек (мелких и глубоких) и двух типов потенциальных барьеров: низких и высо-

ких барьеров для захвата дислокаций в случаях мелких и глубоких ловушек соответственно. С учетом захвата дислокаций в ловушки и выхода из них удалось описать характер деформационного поведения TiAl во всем интервале температур. Получены выражения, которые определяют экстремальные точки на кривой $\sigma_y(T)$. Проанализированы возможные виды зависимости коэффициента упрочнения $\theta(T)$ в области аномальной температурной зависимости $\sigma_y(T)$. Установлены условия, при которых возникает аномальная температурная зависимость $\theta(T)$. Высказано предположение, что форма потенциального рельефа для дислокаций существенно меняется в некоторой области вблизи микротрещины. Захват дислокаций в глубокие ловушки, который стимулируется концентрацией напряжения вблизи микротрещины, и невозможность им покинуть ловушки вплоть до относительно высоких температур рассматривается как возможная причина хрупкости TiAl. Предложена модель, которая описывает деформационное поведение интерметаллидов после некоторой предварительной деформации. Эта модель позволяет описать две альтернативные возможности: наблюдение или отсутствие макроскачка напряжения после указанной деформации.

Запропоновано пояснення немонотонної температурної залежності межі плинності $\sigma_y(T)$ в TiAl, де мають місце два екстремуми, в яких відбувається зміна характеру температурної залежності $\sigma_y(T)$. Порівняння кривих $\sigma_y(T)$ для TiAl та типових кривих для інших матеріалів (ОЦК металів, інтерметалідів типу Ni_3Al) дозволяє реконструювати форму потенціального рельєфу для дислокацій в TiAl. Форма одержаного рельєфу відтворює існування двох типів дислокаційних пасток (мілких та глибоких) та двох типів потенціальних бар'єрів: низьких та високих для захоплення дислокацій відповідно у випадках мілких та глибоких пасток. З урахуванням захоплення дислокацій у пастки та виходу з них вдалося описати характер деформаційної поведінки TiAl в усьому інтервалі температур. Отримано вирази, які дозволяють знайти екстремуми на кривій $\sigma_y(T)$. Проаналізовано можливі типи залежності коефіцієнта зміцнення $\theta(T)$ в області аномальної температурної залежності $\sigma_y(T)$. Встановлено умови, за яких виникає аномальна температурна залежність $\theta(T)$. Висловлено припущення, що форма потенціального рельєфу для дислокацій суттєво змінюється в деякій області поблизу мікротріщини. Захоплення дислокацій в глибокі пастки, яке стимулюється концентрацією напруги поблизу мікротріщини, та неможливість їм покинути ці пастки аж до відносно високих температур розглядається як можлива причина крихкості TiAl. Запропоновано модель, яка описує деформаційну поведінку інтерметалідів після деякої попередньої деформації. Ця модель дозволяє описати дві альтернативні можливості: виникнення або відсутність макрострибка напруги після вказаної деформації.

Key words: TiAl, mechanical properties, yield stress, work hardening rate, flow stress anomaly, brittleness, microstructure, dislocation, Peierls relief, thermally activated blocking.

(Received February 3, 2000)

CONTENTS

1. INTRODUCTION

One generation of intermetallics change another, which is necessitated primarily by the need to have better aerospace materials. Today light-weight titanium aluminides replace intermetallics of the first generation like Ni_3Al and heavy superalloys based on those intermetallics [1, 2]. Titanium aluminides, in the first place TiAl, possess excellent properties [3–5]. Unique complex of physical properties of TiAl includes a high strength/density ratio, heat resistance, high-temperature strength, resistance to oxidation, corrosion and creep, and good fatigue characteristics. But low plasticity of TiAl hampers realization of these properties. Methods for improving TiAl plasticity can be elaborated if we understand causes of deformation strengthening and brittleness of TiAl. This goal is pursued by many researchers, including the authors of this review. The series of titanium aluminides extends further. It includes orthorhombic titanium aluminides based on $Ti_2(Al,Nb)$ [6–8]. They are inferior to TiAl with respect to the strength-density ratio. But their plasticity is better. Elongation about of 16% was achieved for $Ti_2(Al,Nb)$ at room temperature. New problems always arise when one generation of intermetallics replaces another. They include a loss of plasticity when passing from Ni_3Al to TiAl or diffi-

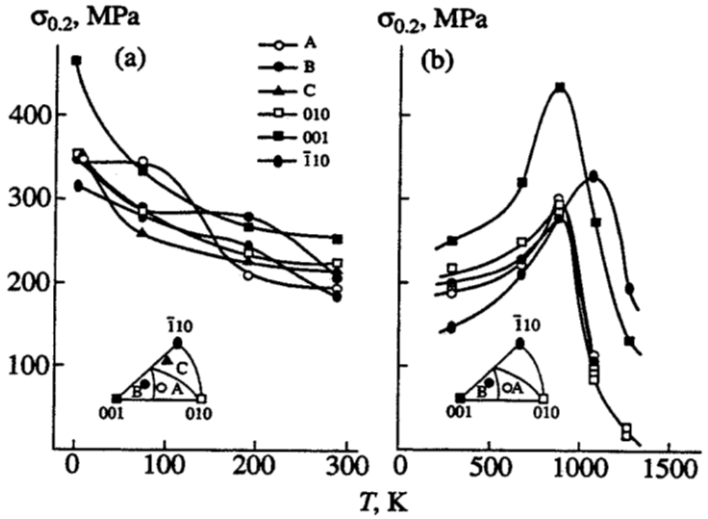

Figure 1. Yield stress of TiAl single crystals in different temperature ranges [9, 10].

culties involved in production of a single-phase material in the case of orthorhombic aluminides, *etc.*

An the interval from room temperature to 600°C. An anomalous dependence anomalous temperature dependence of the yield stress $\sigma_y(T)$, which was inherited from intermetallics of the first generation, should be included in the aforementioned properties of TiAl. The yield stress of TiAl increases in $\sigma_y(T)$ is an excellent property: the higher the temperature, the larger the stress at which plastic flow begins. However, $\sigma_y(T)$ is nonmonotonic for TiAl in the whole temperature interval.

A nonmonotonic temperature dependence of the yield stress $\sigma_y(T)$ in single crystals of TiAl is observed at all orientations (Fig. 1): those favourable for single dislocations and superdislocations [9–11]. The analysis of those data was focused mainly on the anomalous trend of $\sigma_y(T)$. However, the $\sigma_y(T)$ curve has two extrema and, correspondingly, exhibits a normal temperature behaviour in two different temperature intervals (at low and high temperatures) and an anomalous behaviour at intermediate temperatures. Therefore, the nonmonotonic dependence $\sigma_y(T)$ need be interpreted for the whole temperature interval. Moreover, the work hardening rate $\theta(T)$ also has a nonmonotonic dependence, which does not duplicate the dependence $\sigma_y(T)$. Kawabata *et al.* [9] showed that the work hardening rate $\theta(T)$ may have an anomalous trend at some orientations and a normal trend at other orientations in the region of the anomalous behaviour of $\sigma_y(T)$. However, Unui *et al.* [11] noted that even if $\theta(T)$ has an anomalous trend, the temperature of the $\theta(T)$ peak is 100° to 200° lower than the temperature of the $\sigma_y(T)$ peak. One more significant feature of the deformation behaviour of TiAl is a very small strain-rate sensi-

tivity of the flow stress, which is observed [9, 11] in the region of the anomalous behaviour of $\sigma_y(T)$.

In our opinion, the aforementioned features of the deformation behaviour are due to transitions between possible states of dislocations, primarily to thermally activated transitions. The comparison of typical $\sigma_y(T)$ curves observed for various materials made it possible to reconstruct the shape of the potential barrier for dislocations in TiAl. Using those data, we tried to describe the temperature dependence of the deformation characteristics in the whole temperature interval. In addition, assuming that the potential relief for dislocations may change near a crack tip, we made an attempt to explain the brittle–ductile transition in TiAl.

2. TYPICAL $\sigma_y(T)$ CURVES FOR VARIOUS MATERIALS AND TRANSITIONS BETWEEN DISLOCATION STATES

It was proposed [12–15] to describe plastic deformation as an evolution of a dislocation population, which is determined by multiplication of dislocations and their transformations. These processes occur on the background of elastic stress fields created by the dislocation ensemble itself. The transformations actually represent transitions between possible states of dislocations. It is reasonable to think that dislocations are 'born' glissade. If the energy of a dislocation in the glissade (g) form is larger than in the sessile (s) form, g→s transformations are possible. During these transformations a gain in the dislocation energy is achieved at the expense of a loss of mobility by dislocations. Reverse s→g transformations, which return dislocations to the glissade form, are usually thermally activated. Direct g→s transformations may be either thermally activated or athermal. It is necessary to distinguish thermally activated processes among g↔s transformations. It is these processes that determine the temperature dependence $\sigma_y(T)$.

Figure 2 presents typical $\sigma_y(T)$ curves for some materials. A possible potential relief, *i.e*. the potential energy of various dislocation states, is sketched schematically in a simplest form for the same materials in Fig. 3.

Since the energy of the glissade form of dislocations is higher than the energy of the sessile form, the potential barrier separating these states is asymmetric: the potential well for the glissade form is shallower than the well for the sessile form.

Metals having a b.c.c. lattice are characterized by a sharp drop of $\sigma_y(T)$ with growing temperature [16]. It is assumed to be an established fact that planar and non-planar configurations of the wide core of dislocations represent g- and s-states respectively in b.c.c. metals [17]. It is the thermally activated s→g transition that determines the observed dependence $\sigma_y(T)$. But the g→s transition is not a thermally activated one. Otherwise, $\sigma_y(T)$ would have an anomalous trend, which would change to the normal trend with growing temperature.

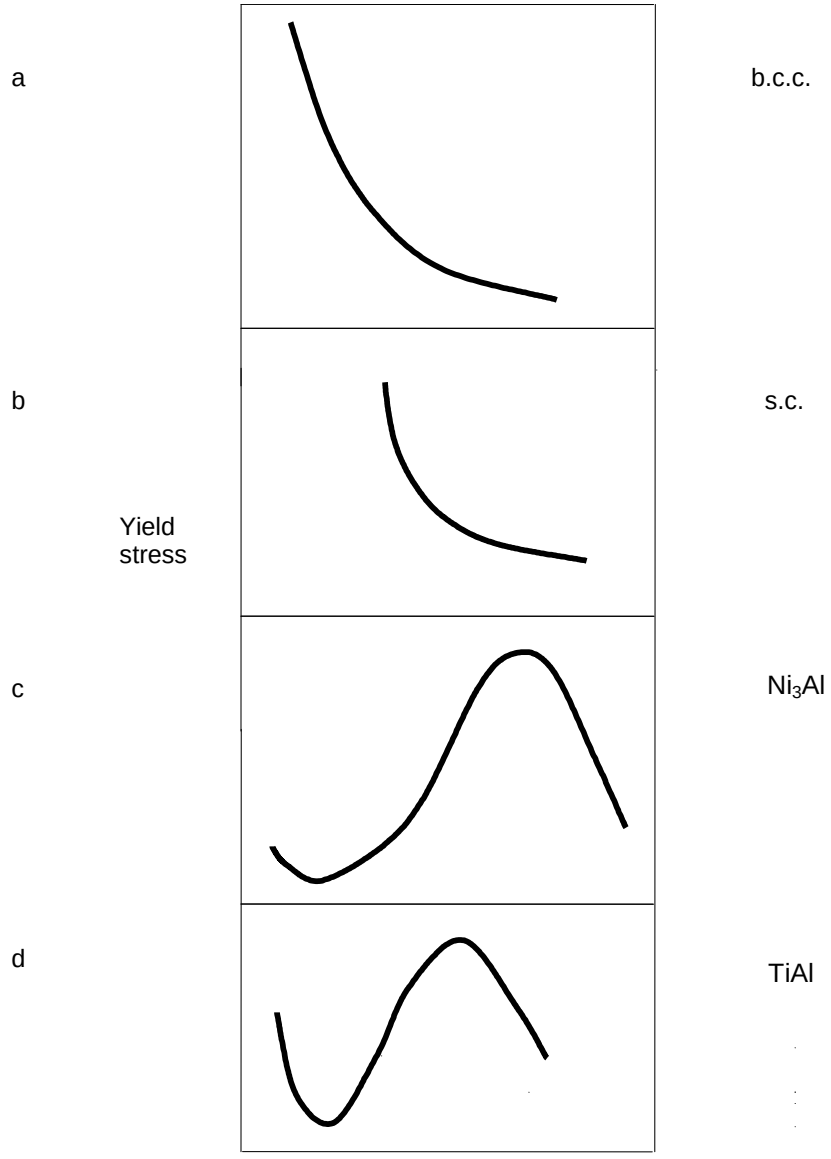

Figure 2. Typical $\sigma_y(T)$ curves for some materials: a—b.c.c. metal; b—semiconductor; c—Ni_3Al intermetallic; d—TiAl intermetallic.

A typical feature of semiconductors is that plastic flow is first observed at relatively high temperatures, and $\sigma_y(T)$ exhibits a normal trend [18]. In the given case g→s′ transitions are due to immersion of a dislocation into a deep Peierls valley.

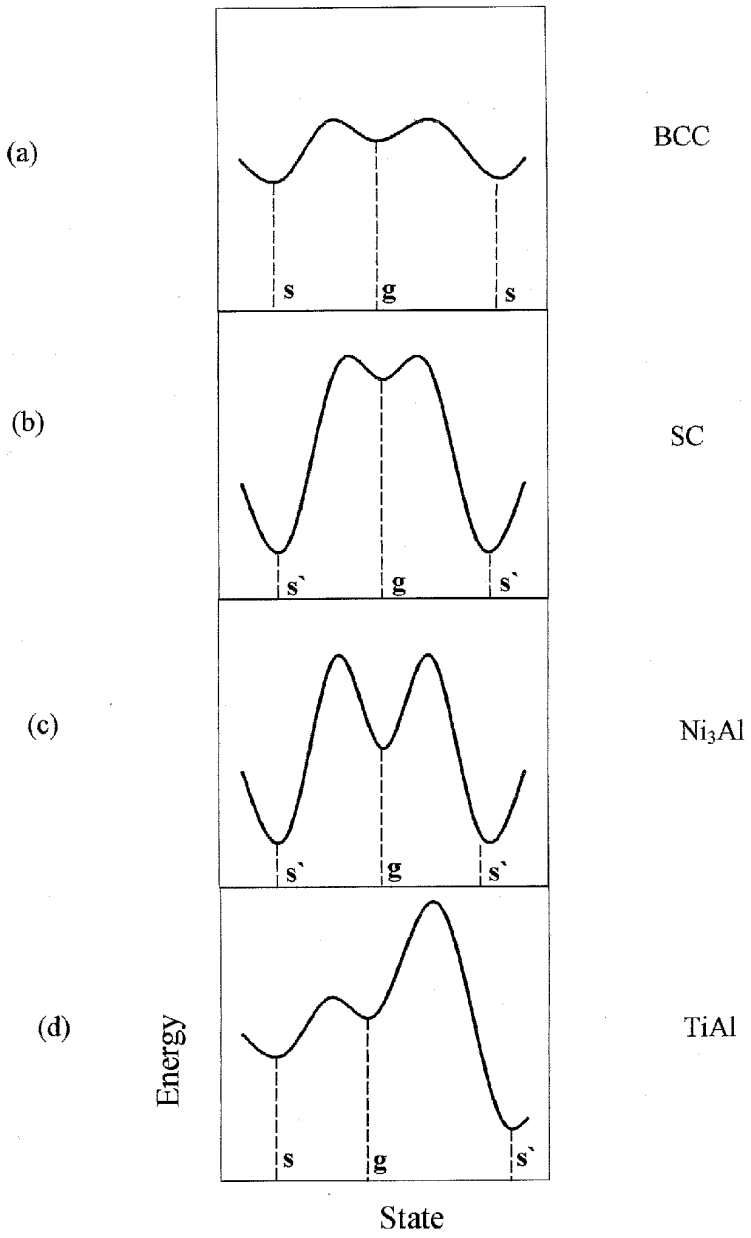

Figure 3. Schematic picture of potential relief for dislocation in different materials; g—glissade state; s, s′—sessile state.

In both cases (Fig. 3a, 3b), the potential well of the g-state is so shallow that thermal activation is unnecessary to escape this potential well.

Here the potential well is conditional only. The potential well for the s′-state (Fig. 3b) is much deeper than for the s-state (Fig. 3a). Therefore s′→g transitions are possible only at relatively high temperatures, a fact which determines the observed temperature dependence $\sigma_y(T)$ in semiconductors.

Such intermetallics as Ni_3Al are characterized by the $\sigma_y(T)$ curve having the shape shown in Fig. 2c: a weak normal dependence at low temperatures (region I); an anomalous trend at intermediate temperatures (region II); a normal trend at high temperatures (region III) [1, 2]. A non-monotonic temperature dependence $\sigma_y(T)$ with two extrema, which is observed for TiAl, is shown schematically in Fig. 2d. A specific feature of the $\sigma_y(T)$ curve for TiAl is that the temperature drop at low temperatures is much larger than for Ni_3Al.

The observed temperature dependence $\sigma_y(T)$ can be explained if one assumes that the potential relief for dislocations is more complicated in intermetallics than in the aforementioned simple materials. What is meant here is that intermetallics contain, in addition to one type (g) of glissade dislocations, two types of sessile dislocations, which correspond to shallow (s) and deep (s′) potential wells. Dislocations move for some time on the relief with shallow wells, which allows some free path length λ, and then 'fall' into a deep well. To emphasize this feature of the relief, shallow wells would be repeated several times in the sketch diagram of the relief for Ni_3Al (Fig. 3c) and TiAl (Fig. 3d).

Wells of the s-type prove to be very shallow in Ni_3Al. Barriers separating these wells are easily surmounted and the relief has little effect on the temperature dependence of the yield stress even at low temperatures. Deep wells of the s′-type correspond to a blocked Kear–Wilsdorf configuration. As is known [19], such barriers appear due to resplitting of a superdislocation when a superpartial dislocation goes to the cube plane (Fig. 4a). As distinct from g→s transitions, a relatively high potential barrier need be surmounted for g→s′ transitions (see Fig. 3c), which are realized by a thermally activated mechanism. These transitions take a long waiting time, during which a dislocation undergoes a number of g↔s transitions.

Note also a large asymmetry of the potential barrier separating g- and s′-type states. This leads to a rigorous relation between activation energies of forward (g→s′) and reverse (s′→g) transitions: $U_{gs'} < U_{s'g}$ Consequently, g→s′ transitions determine an anomalous trend of $\sigma_y(T)$ in the region II, and s′→g transitions are responsible for the normal trend of $\sigma_y(T)$ in the region III.

Let us analyse the character of the presumed potential relief for a dislocation in TiAl (Fig. 3d). The main distinction from the situation discussed above (Fig. 3c) is that potential wells of the s-type are not so shallow in TiAl as in Ni_3Al. Consequently, thermal activation is required to escape these potential wells. This determines a sharp drop of $\sigma_y(T)$ with temperature in the region I. When temperature is increased, dislocations may go to the s′-state by a thermally activated mechanism. Similarly to

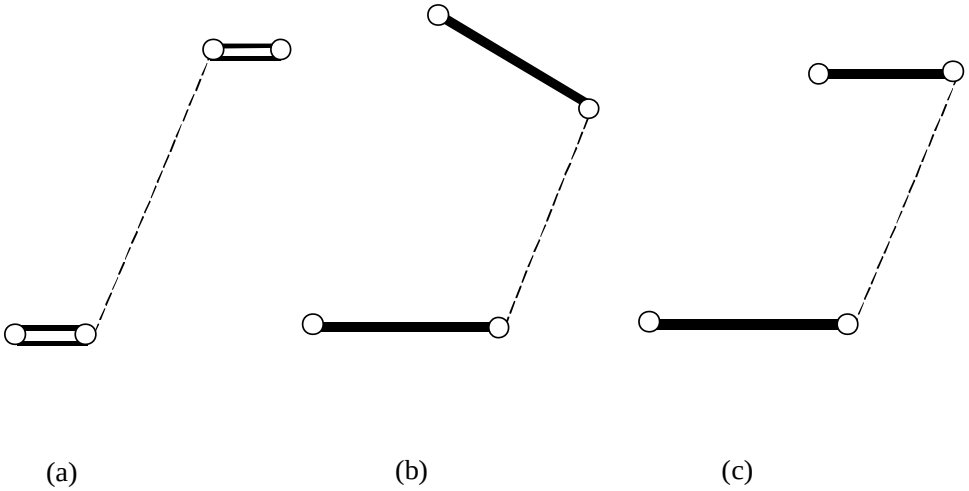

Figure 4. Schematic picture of Kear–Wilsdorf barrier: a—Ni_3Al, b, c—TiAl; double line—complex stacking fault, bold line—superstructural stacking fault, dotted line—{010} APB.

the case considered above, the transition takes a long waiting time, during which movement of a dislocation is connected with potential wells of the s-type.

Consider first a single dislocation. It is assumed that g→s′ transitions are connected with submersion of a dislocation in deep Peierls valleys [20]. One can expect a potential well of the s′-type to be deep as in semiconductors (Fig. 3b). Then a question arises: which main g-state should single dislocations in TiAl have so that their blocking in deep Peierls valleys requires, unlike in semiconductors, thermal activation and causes an anomalous trend of $\sigma_y(T)$. Moreover, the choice of the main state determines the reason why an anomalous trend of $\sigma_y(T)$ is replaced by the normal trend at low temperatures.

A single dislocation in the main g-state is supposed not to be constricted but to have a wide planar core [21]. In this case transitions of two types, g→s and g→s′, are possible from the main state. Put another way, a potential well corresponding to the g-state in TiAl has walls of different height: a low wall for the g→s transition to an non-planar wide core and a high wall for the g→s′ transition to a constricted dislocation localized in a deep Peierls valley. Only g→s′ transitions are thermally activated, because they require formation of a constriction as a necessary step. Therefore blocking of a single dislocation in deep Peierls valleys occurs through thermal activation rather than spontaneously.

Thus, at orientations favourable for single dislocations, a non-monotonic dependence $\sigma_y(T)$ is determined by the following thermally ac-

tivated transformations: the normal trend at low temperatures (region I) depends on s→g transformations of a wide non-planar core to a planar core; an anomalous trend at intermediate temperatures (region II) is due to g→s′ transformations of a wide core to a constricted form localized in a deep Peierls valley; the normal trend at high temperatures (region III) is determined by s′→g processes of the dislocation release from a deep Peierls valley.

Similarity of the curves describing a nonmonotonic behaviour of $\sigma_y(T)$ in TiAl at different orientations is observed. The analysis of numerous TEM data suggests some feature in common for a single dislocation and a superdislocation or, more precisely, the constituent 1/2⟨101] superpartial dislocation: no band of a complex stacking fault is observed in both cases [22]. It seems reasonable to assume that the superpartial dislocation has, like a single dislocation, a wide core. But the core of the 1/2⟨101] superpartial dislocation differs structurally from the core of a single dislocation. This is because an APB band borders on the superpartial dislocation and couples it to an adjacent partial dislocation.

Thus, a ⟨101]-superdislocation in the main g-state has a glissade configuration, which includes a superpartial dislocation with a wide planar core. Similarly to a single dislocation, transitions of two types, g→s and g→s′, are possible for a superdislocation in the main state. The potential well corresponding to the g-state has walls of different height (Fig. 3d): a low wall and a high wall for g→s and g→s′ transitions respectively. The g→s transition describes rearrangement of the wide core of a superpartial dislocation from a planar to a non-planar form, while the g→s′ transition gives rearrangement of a glissade superdislocation caused by its resplitting (Figs. 4b, c). The analogy readily transpires to the g→s′ transformation of a glissade superdislocation to a blocked Kear–Wilsdorf configuration in Ni_3Al discussed earlier. Referring to g→s transitions in TiAl, they are largely similar to rearrangement of the wide core of a superpartial dislocation in Pt_3Al [23].

Consequently, at orientations favourable for superdislocations, a nonmonotonic dependence $\sigma_y(T)$ is determined by the following thermally activated transformations: the normal trend at low temperatures (region I) depends on s→g transformations of the wide core of a superpartial dislocation from an non-planar to a planar form; an anomalous trend at intermediate temperatures (region II) is due to g→s′ transformations of a superdislocation to a blocked form as a result of resplitting; the normal trend at high temperatures (region III) is determined by s′→g transformations of a superdislocation from a blocked to a glissade form. Although this sequence of transformations describes rather fully, as shown later, the observed dependence $\sigma_y(T)$, the actual picture is more complicated, because two types of superdislocations exist: some are not observed in the region II and others in the region III. Causes of their vanishing will be discussed in section 3.4 below.

The form of the potential relief described above is rough. In actual fact,

the potential relief exists in a multidimensional configuration space. One can say only about plane sections of the potential relief depending on which co-ordinates characterizing the state of a dislocation are fixed. Moreover, an energy barrier is characterized by its shape in addition to the wall height. It is essential whether the barrier walls are steep or not. However, the proposed approach can be used as the first approximation.

3. DESCRIPTION OF A NONMONOTONIC TEMPERATURE DEPENDENCE $\sigma_y(T)$

Let us derive expressions that determine the yield stress in each of the three temperature intervals for the presumed form of the potential relief in TiAl (Fig. 2d).

3.1. Low-Temperature Drop of $\sigma_y(T)$

The plastic deformation equation (allowing also for the elastic part of deformation) for a population, which includes dislocations in g- and s-states, can be written as [13–15]:

$$\frac{1}{\mu^2}\frac{d\sigma^2}{d\varepsilon} = \varepsilon_c\left(1 - \frac{1}{\mu}\frac{d\sigma}{d\varepsilon}\right) - \frac{1}{\mu^2}\frac{\sigma^2}{\varepsilon_s}\,, \tag{1}$$

where dimensionless quantities ε_c and ε_s denote characteristic deformations. They have the form

$$\varepsilon_c = \alpha^2 f^{-3} b\lambda_{gs}^{-1} \quad \text{and} \quad \varepsilon_s = \dot{\varepsilon} / \nu_{sg}\,. \tag{2}$$

Here λ_{gs} is the free path length connected with g→s transformations; ν_{sg}—the frequency of s→g transformations; *b*—the Burgers vector magnitude; μ—the shear modulus; *f*—the Schmid factor for the given slip system; α denotes some numerical coefficient. The second term in brackets describes the contribution from the elastic part of deformation. It tends to unity in the region of elastic deformation and to zero in the region of plastic deformation.

The notation (1) assumes that sources of dislocations operate rapidly and adjust the applied stress to the density of dislocations ρ in accordance with the known relation

$$\sigma = \kappa\sqrt{\rho} \quad \text{and} \quad \kappa = \alpha\mu b / f\,. \tag{3}$$

In addition, the initial density of dislocations is taken to be small. We shall not consider the case of slow operation of sources and, correspondingly, a finite time of adjustment between ρ and σ, when it is necessary to introduce an equation for the population growth by multiplication of disloca-

tions [13–15].

The relative contribution of the terms in equation (1) is determined by the relation between the lifetime of the s-state ν^{-1}_{sg} and the observation time $\varepsilon / \dot{\varepsilon}$. In the limiting case, when $\nu^{-1}_{sg} << \varepsilon / \dot{\varepsilon}$, *i.e*. the s-state is a short-lived one, the relation

$$\frac{d\sigma}{d\varepsilon} << \frac{\sigma}{\varepsilon} \frac{\varepsilon / \dot{\varepsilon}}{\nu^{-1}_{sg}}, \tag{4}$$

is fulfilled.

Therefore, in accordance with (1), the work hardening rate in the region I is small and the yield stress σ^{I}_{y} is determined by the expression

$$\frac{\sigma^{I}_{y}}{\mu} = \sqrt{\varepsilon_s \varepsilon_c}\,. \tag{5}$$

It is assumed that only s→g transformations are thermally activated in the region I (see section 2). Therefore

$$\nu_{sg} = \tilde{\nu}_{sg} \exp\left(-\frac{U_{sg}}{kT}\right), \tag{6}$$

where U_{sg} is the activation energy of the s→g transformation.

Taking into account (2) and (6), the expression (5) readily yields

$$\sigma^{I}_{y} = \tilde{\sigma}^{I}_{y} \exp\left(-\frac{U_{sg}}{2kT}\right). \tag{7}$$

Here $\tilde{\sigma}^{I}_{y}$ changes with $\sqrt{\dot{\varepsilon}}$, because ε_s is proportional, in accordance with (2), to $\dot{\varepsilon}$. However, expression (7) holds only if one assumes that quantities ε_c and ε_s are independent of the stress. Otherwise, expression (5) should be considered as an equation for determination of σ^{I}_{y}. If the stress dependence of the activation energy U_{sg} is taken into account, σ^{I}_{y} exhibits a weaker dependence on temperature and strain rate [13, 15]. The normal temperature trend of $\sigma^{I}_{y}(T)$ is preserved. This situation will not change until thermally activated g→s′ transformations, which cause blocking of dislocation sources, become significant.

3.2. Anomalous Temperature Trend of $\sigma_y(T)$

In many cases specific features of the deformation behaviour of TiAl stem from one and the same reason: thermally activated blocking of dislocation sources. A direct consequence is an anomalous temperature dependence $\sigma_y(T)$. One more obvious consequence is the aforementioned vanishing of dislocations of definite type in some temperature intervals as discussed below. Less obvious but nonetheless significant are conse-

quences of dislocation source blocking, which is initiated by some external effect. Such unexpected consequences include, in the final analysis, brittleness of TiAl (see section 4) and stress macrojump (see section 5).

3.2.1. Thermally activated blocking of dislocation sources

A dislocation source can operate if a dislocation segment passes the critical configuration before it is blocked. As a result, the free path length, λ_F, of a dislocation belonging to a source serves as the maximum linear dimension of the source [24–26]. A segment, whose length exceeds λ_F, becomes blocked rather than acquires the critical configuration. In other words, the source will not operate. For plastic flow to begin, the applied stress should be higher than the characteristic minimum value of the switch-on stress σ_F of a dislocation source, which is connected to the length λ_F, by the relation

$$\sigma_F f = \mu b/\lambda_F. \tag{8}$$

Here and henceforth the index *F* refers to quantities associated with dislocation sources. The introduction of σ_F as a threshold value determining the behaviour of a dislocation population does not mean that plastic flow is prohibited in principle at stresses lower than σ_F. One should allow for smearing of the switch-on stress σ_F. This is due to both the statistical character of thermally activated processes and fluctuating character of the internal stress field. Similarly, another threshold stress—the stress determined by (1) and needed to overcome the elastic counteraction of the dislocation framework—is smeared too. Smearing of these threshold stresses can be taken into account by the method proposed in Refs. [14, 15].

In the case of the thermally activated g→s′ transformation $\lambda_F(T)$ can be written as

$$\lambda_F = \tilde{\lambda}_F \exp\left(U^F_{gs'} / (kT)\right), \tag{9}$$

where $U^F_{gs'}$ is the blocking activation energy of a dislocation belonging to a source. From (8) and (9) it follows that

$$\sigma_F(T) = \tilde{\sigma}_F \exp\left(-\frac{U^F_{gs'}}{kT}\right), \tag{10}$$

Assuming that the yield stress $\sigma^{II}_y(T)$ is determined by the switch-on stress of a dislocation source $\sigma_F(T)$, from (10) we immediately obtain an anomalous temperature dependence of the stress $\sigma^{II}_y(T)$. Let it be emphasized that expressions (8) and (10) proceed from the assumption that in

the region II the s′-state of a dislocation belonging to a source is long-lived and activation energies are interrelated as $U^F_{gs'} < U^F_{s'g}$. From (7) and (9) it is seen that $\sigma^{II}_y(T)$ is independent of the strain rate $\dot{\varepsilon}$. As stated earlier, the strain-rate sensitivity of the flow stress, which is observed in the region II, is weak indeed.

3.2.2. Temperature dependence of the work hardening rate

From (9) it is seen that the source switch-on stress $\sigma_F(T)$ drops with decreasing temperature. At sufficiently low temperatures $\sigma_F(T)$ becomes smaller than $\sigma_y(T)$, which is determined by (5), and can be neglected. However, $\sigma_F(T)$ should outgrow $\sigma^I_y(T)$ with increasing temperature, because these quantities have different temperature trends. The region II of an anomalous temperature dependence of the yield stress starts at temperatures when $\sigma_F(T) > \sigma^I_y(T)$. Thus, the temperature of the minimum, $T_{\min}$, in the $\sigma_y(T)$ curve for TiAl is determined by the equation

$$\frac{\sigma_F(T_{\min})}{\mu} = \sqrt{\varepsilon_s \varepsilon_c}\ . \tag{11}$$

Write the equation of plastic deformation allowing for g↔s′ transformations in the form analogous to (1):

$$\frac{1}{\mu^2}\frac{d\sigma^2}{d\varepsilon} = \varepsilon_{c'} - \frac{\sigma^2}{\mu^2}\frac{1}{\varepsilon_{s'}}\ , \tag{12}$$

where

$$\varepsilon_{c'} = \alpha^2 f^{-3} b \lambda^{-1}_{gs'} \quad \text{and} \quad \varepsilon_{s'} = \dot{\varepsilon} / \nu_{s'g}\ . \tag{13}$$

If both g↔s′ transformations are thermally activated, we have

$$\lambda_{gs'} = \tilde{\lambda}_{gs'} \exp\left(\frac{U_{gs'}}{kT}\right),$$
$$\nu_{s'g} = \tilde{\nu}_{s'g} \exp\left(-\frac{U_{s'g}}{kT}\right). \tag{14}$$

In equation (12) the first term in the right-hand side describes blocking of dislocations owing to g→s′ transformations, while the second term gives unblocking of dislocations as a result of s′→g transformations. As distinct from (1), the first term in (12) does not include a factor allowing for elastic deformation. Equation (12) holds only when $\sigma \geq \sigma_F(T)$ and elastic part of deformation, for which $\sigma = \mu\varepsilon$, extends up to ε values equal to $\varepsilon_F = \sigma_F(T)/\mu$ and it is omitted from this equation. Thus, initial values for equation (12) are $\sigma = \sigma_F(T)$ and $\varepsilon = \varepsilon_F$, where $\sigma_F(T)$ is determined by expression (10). At the beginning of deformation, when the flow stress is still close to $\sigma_F(T)$,

equation (12) can be written in the form:

$$\frac{1}{\mu}\frac{d\sigma}{d\varepsilon} = \frac{\varepsilon_{c'}}{2\sigma_F}\mu\left(1 - \frac{\varepsilon_F^2}{\varepsilon_{s'}\varepsilon_{c'}}\right). \tag{15}$$

Let us consider the case when blocked configurations of the s′-type are practically indestructible and the second term on the right of (15) can be neglected. This case corresponds to moderate temperatures. From (15) we have

$$\frac{d\sigma}{d\varepsilon} \cong \theta, \quad \frac{\theta}{\mu} = \frac{\varepsilon_{c'}}{2\varepsilon_F}. \tag{16}$$

Hence, considering (10), (13) and (14), we obtain

$$\theta = \tilde{\theta}\exp\left(-\frac{U_{gs'} - U^F_{gs'}}{kT}\right). \tag{17}$$

From (17) it is seen that $\theta(T)$ is independent of temperature if activation energies are nearly equal, *i.e*. $U_{gs'} \cong U^F_{gs'}$. The fact that the temperature dependence of the work-hardening rate $\theta(T)$ is indeed observed is an evidence that blocking of dislocations at the stage of multiplication and during subsequent deformation has different activation energies $U^F_{gs'}$ and $U_{gs'}$ respectively. From (17) it follows that the relation $U^F_{gs'} < U_{gs'}$ should be fulfilled for the coefficient $\theta(T)$ to have an anomalous temperature dependence. This relation seems to be reasonable, because a dislocation belonging to a source can be blocked easier than in the bulk thanks to the presence of pinning points. If $U_{gs'} > 2U^F_{gs'}$ a coefficient $\theta(T)$ exhibits a stronger temperature dependence than $\sigma_y(T)$. If $U^F_{gs'} < U_{gs'} < 2U^F_{gs'}$, the temperature dependence $\theta(T)$ is weaker than that of $\sigma_y(T)$. The observed types of the temperature dependence $\theta(T)$ [9] are illustrated in Fig. 5.

3.3. Drop of $\sigma(T)$ Above the Temperature Peak

When the temperature rises, s′→g transformations become significant and can determine the onset of plastic flow. In this case, $\sigma_y(T)$ can be presented as σ_y^{III}, which is given by an expression analogous to (5):

$$\frac{\sigma_y^{III}}{\mu} = \sqrt{\varepsilon_{s'}\varepsilon_{c'}}. \tag{18}$$

Taking into account (13) and (14), from (18) we have

$$\sigma_y^{III} = \tilde{\sigma}_y^{III}\exp\left(\frac{U_{s'g} - U_{gs'}}{2kT}\right). \tag{19}$$

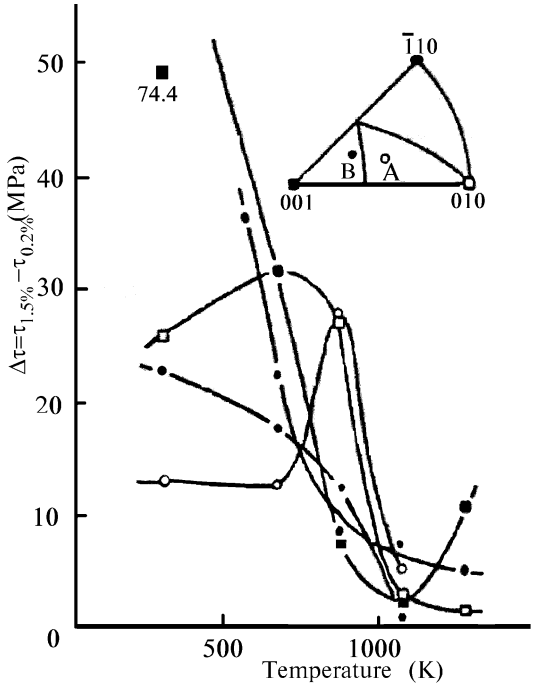

Figure 5. Temperature and orientation dependence of work hardening rate [9].

If the stress dependence of the activation energy is neglected, it readily follows that σ_y^{III} depends, unlike σ_F, on $\dot{\varepsilon}$, namely $\propto \sqrt{\dot{\varepsilon}}$, and exhibits a normal temperature behaviour, because the obvious condition $U_{gs'} < U_{s'g}$ is fulfilled (see section 2). Thus, growth of the yield stress with increasing temperature should be followed by its drop described by expression (19). In this case the temperature T_{max} of the maximum in $\sigma(T)$ is found from the equation

$$\sigma_F(T_{max}) = \sigma_y^{III}(T_{max}), \tag{20}$$

which can be written as

$$\varepsilon_F = \sqrt{\varepsilon_{s'}\varepsilon_{c'}}\ . \tag{21}$$

From (15) and (20) it is seen that the work hardening rate $\theta(T)$ decreases near the temperature T_{max} and turns to zero at $\theta = T_{max}$. This means that $\theta(T)$ passes its maximum at a lower temperature than $\sigma_y(T)$ does. Put another way, the $\theta(T)$ peak is shifted relative the $\sigma_y(T)$ maximum towards lower temperatures. As stated earlier [11], this behaviour of the deformation characteristics indeed is observed both for TiAl and other intermetallics.

When $T > T_{max}$, the upper and lower yield stress exists at high temperatures in TiAl [9,11] as in semiconductors. Expression (19) just determines the lower yield stress σ_y^L. If the stress dependence of the activation energy is taken into account, weaker temperature and rate dependencies of σ_y^L can be obtained as for σ_y^L considered above. The presence of the upper yield stress σ_y^U indicates [13–15] that the characteristic time τ of dislocation multiplication, *i.e*. the switch-on time of dislocation sources and, correspondingly, the time required for adjusting ρ and σ, is relatively long. The analysis of the equation for the dislocation population growth during slow operation of dislocation sources showed that the upper yield stress is proportional to $\dot{\varepsilon}\tau$.

Eventually, the deformation behaviour of TiAl is different in regions I and III, because potential wells corresponding to s- and s′-states have different depth (see Fig. 3d). Therefore two types of traps exist: shallow traps of the s-type and deep traps of the s′-type. Release of dislocations from traps leads to a normal temperature dependence $\sigma_y(T)$. It is quite reasonable that the drop of $\sigma_y(T)$ with growing temperature in regions I and III is due to release of dislocations from shallow and deep traps respectively.

However, the presence of two types of traps is insufficient for the observed trend of $\sigma_y(T)$. Dislocations should first be captured in these traps. Assume that a potential well corresponding to the g-state has walls of the same height as for transition to s- and s′-type states. In this case TiAl would exhibit a different deformation behaviour. Indeed, s-type traps would be unobservable, because g→s′ transitions to the long-lived state always dominate over g→s transitions to the short-lived state at comparable free path lengths of dislocations [27]. The density of blocked s′-type dislocations actually is much higher than the density of blocked s-type dislocations, because s′-type dislocations accumulate during the whole observation time equal to $\varepsilon/\dot{\varepsilon}$, while s-type dislocations accumulate only during their lifetime $\nu_{sg}^{-1} << \varepsilon/\dot{\varepsilon}$. But, then, a strong drop of $\sigma_y(T)$ with growing temperature in region I would be unobservable. The more so that s-type traps would not have any effect on the deformation behaviour of TiAl if the barrier for g→s transitions is higher than the barrier for g→s′ transitions. Only when the barrier for g→s transitions is lower than for g→s′ transitions, both types of traps show up themselves: shallow traps in region I, and deep traps in regions II and III. The origin of deep traps is different for dislocations of various types: they result from immersion of single dislocations to deep Peierls valleys, whose presence is due to covalent-like interatomic bonds, and resplitting of superdislocations, which is followed by formation of low-energy surface defects.

3.4. Evolution of the Dislocation Structure with Temperature

TEM investigations of the dislocation structure of TiAl helped ascertaining

types of dislocations observed in various temperature intervals and forms (glissade or blocked) of dislocations [28–34]. Vanishing of superdislocations 1/2⟨112] at intermediate temperatures (region II) and superdislocations ⟨101] at high temperatures (region III) was noted. We relate this effect to thermally activated blocking of dislocation sources.

If a population comprises dislocations of different types, plastic flow will be realized by dislocations whose sources are switched on at a lower stress σ_F. Sources, which can be easily blocked (the activation energy $U^F_{gs'}$ is small), will not be switched on and dislocations of the corresponding type will be unobservable. It may be thought that easy recombination of a superpartial dislocation causes blocking of 1/2⟨112] superdislocations. Indeed, calculations [32]. suggest that the wide core of a superpartial dislocation will be constricted due to the stress field of an adjacent partial dislocation. This stress field will favour blocking of sources of 1/2⟨112] superdislocations. Consequently, 1/2⟨112] superdislocations are unobservable in the region II. This example is also significant as direct evidence that the stress field may stimulate blocking of dislocation sources.

However, superdislocations 1/2⟨112] can be made observable in region II by the following method [32]: deformation at −196°C and weak deformation *in situ* at 300°C. Superdislocations 1/2⟨112] are injected during low-temperature deformation, when sources are not blocked, and become blocked after deformation *in situ*. A blocked superdislocation 1/2⟨112] is shown in Fig. 6.

Moreover, the following situation may arise: $s' \rightarrow g$ transformations are already realized for dislocations of some type, while blocked configurations remain indestructible for dislocations of another type. The switch-on stress σ_F of the last type of dislocations will continue growing with increasing temperature in accordance with (10).

Plastic flow will start at a smaller stress, which is connected with $g \leftrightarrow s'$ transformations and decreases with temperature in accordance with (19). One may think that this situation is realized in region III where ⟨101] superdislocations are unobservable [29, 32]. In the final analysis, this is explained by indestructibility of blocked superdislocations of the Kear–Wilsdorf type in TiAl. These blocked superdislocations cannot be easily transformed to glissade configurations, because it is difficult to constrict the band of a superstructural stacking fault. The ⟨101] superdislocations may be observed at high temperature as product of dislocation reactions only. Therefore the drop of $\sigma_y(T)$ in region III is due to unblocking of single dislocations or 1/2⟨112] superdislocations.

Figure 7 shows a dislocation structure with blocked dislocations after deformation at −196°C. Microphotographs of superdislocations blocked at intermediate temperatures are given in Fig. 8.

A typical microphotograph [31] shows a configuration, which we referred to as ‘a tree’, was observed more than once [33]. The trunk of the

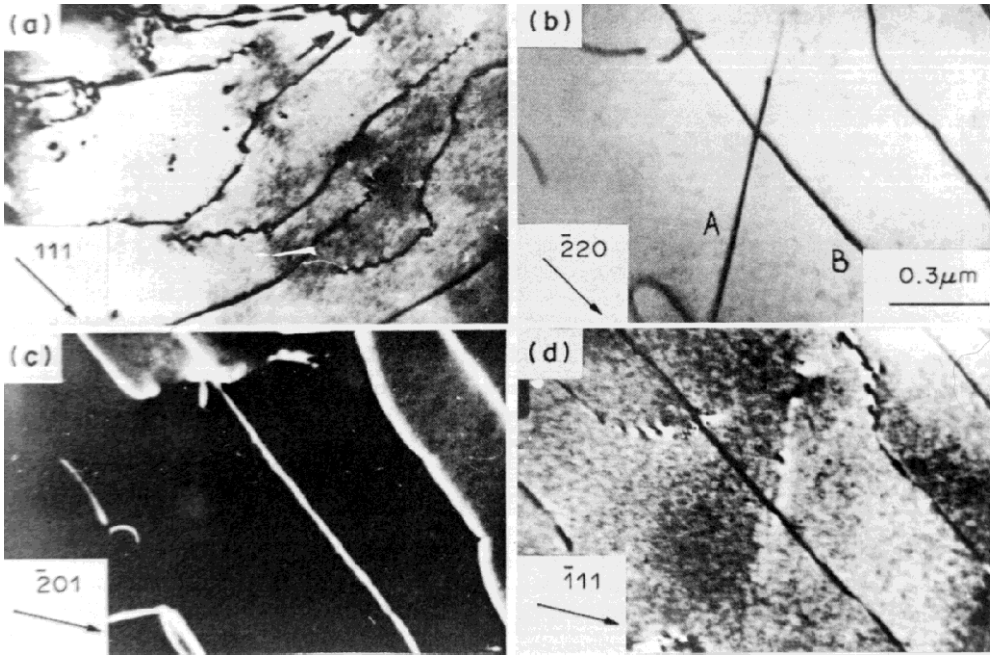

Figure 6. Dark-field electron micrographs [32] taken from a sample of Ti–50Al alloy deformed at −196°C (a) and after two-stage treatment (b–d): beam direction BD near [110]; Burgers vectors of dislocations A and B are $1/2[1\,\bar{1}\,2]$ and $1/2[\bar{1}\,10]$ respectively.

tree is a blocked superdislocation in the form of a Kear–Wilsdorf barrier and branches are represented by single dislocations. Single dislocations blocked at intermediate temperatures are seen in Fig. 9. The fact that blocked dislocations are observed both at very low [10, 34] and relatively high temperatures confirms the above supposition on two types of traps. Microstructure of TiAl after high temperature deformation is shown in Fig. 10.

Typical microphotograph of blocked single dislocations is presented in Figs. 9a, 9b. A clearly pronounced rectilinearity of long segments of single dislocations is remarkable [30, 31]. Figure 9c depicts two families of blocked single dislocations having mutually perpendicular Burgers vectors. However, single dislocations having a number of pinning points with bent segments between those points were observed too [11, 35, 36]. But mostly they extended along their Burgers vector (Fig. 9d). A paradoxical situation arises: on the one hand, $\sigma_y(T)$ and $\theta(T)$ exhibit an anomalous trend and, on the other hand, TEM data suggest possible unblocking of single dislocations at intermediate temperatures.

The microstructure in Fig. 9d can be interpreted as follows. Single dislocations emitted by a source are localized in deep valleys. Subsequently double kinks can be formed. Screw segments of these double kinks

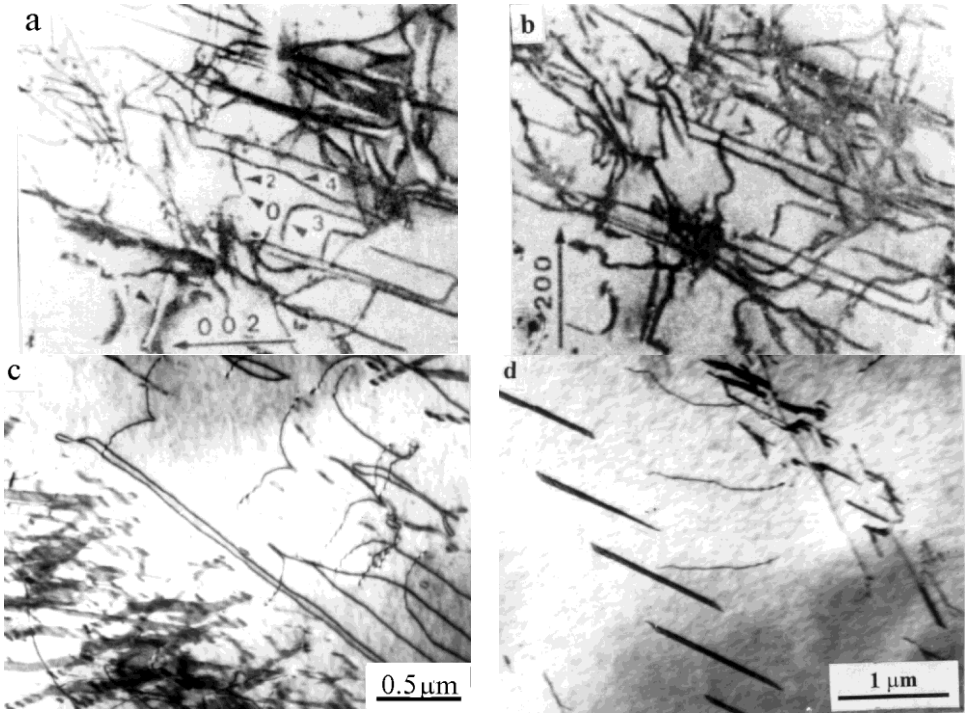

Figure 7. Microstructure of TiAl at −196°C: a, b—dark-field images of dislocations in Ti–56Al [10]; c, d—bright-field images of dislocations in Ti–50Al (courtesy O. V. Antonova and N. V. Kazantseva).

again are localized in deep valleys. When Schmid factors of a single dislocation are equal in both octahedral planes, double kinks can be emitted in these planes. A node in a single dislocation, where such kinks meet one another, serve as a pinning point. Therefore observation of pinning points is only the sign accompanying above—mentioned transitions of a single dislocation.

The situation is fully described by expression (10) and Eq. (12). Expression (10) gives an anomalous trend of $\sigma_F(T)$ and, correspondingly, $\sigma_y(T)$. As the degree of deformation increases and the flow stress exceeds σ_F, the second term on the right of Eq. (12), which describes s′→g transformations (or unblocking of dislocations), grows. However, as long as the condition $\varepsilon_{s'}\varepsilon_{c'} > \varepsilon_F^2$ is fulfilled, an anomalous trend of $\theta(T)$ will continue.

Thus, the cause of an apparent discrepancy between TEM data and observed anomalies is that the characteristic time of dislocation multiplication is much shorter than $\varepsilon/\dot{\varepsilon}$.

Therefore s′→g transformations, which were not realized during dislocation multiplication, become possible upon subsequent plastic deforma-

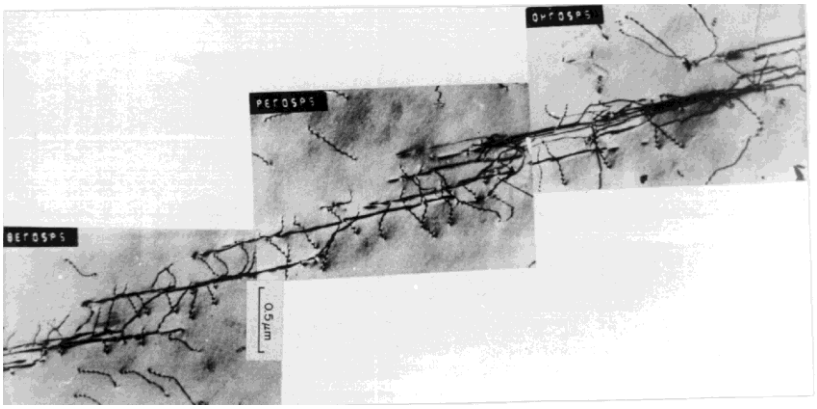

Figure 8. Bright-field images of the dislocation configuration (‘tree’) in a sample of Ti–50Al alloy after deformation at 400°C [31].

tion. Elementary events of unblocking are observed in an electron microscope.

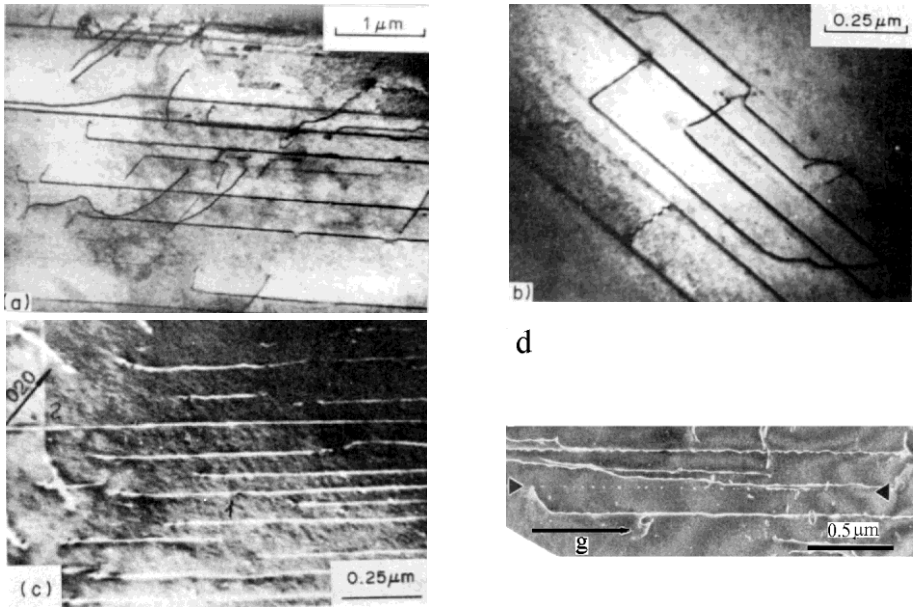

Figure 9. TEM images of single dislocations at intermediate temperature: a, b—microstructure of Ti–50Al alloy deformed at 400°C [31]; c—dark-field electron micrographs [32] taken from a Ti–50Al sample deformed at 540°C; two families of blocked screw dislocations with Burgers vectors: 1—1/2[$1\bar{1}0$], 2—1/2[110], recorded with **g** = [020]; d—single dislocation in a sample of γ-$Ti_{47}Al_{51}Mn_2$ alloy deformed at 500°C, **g** = [$\bar{2}20$] [35].

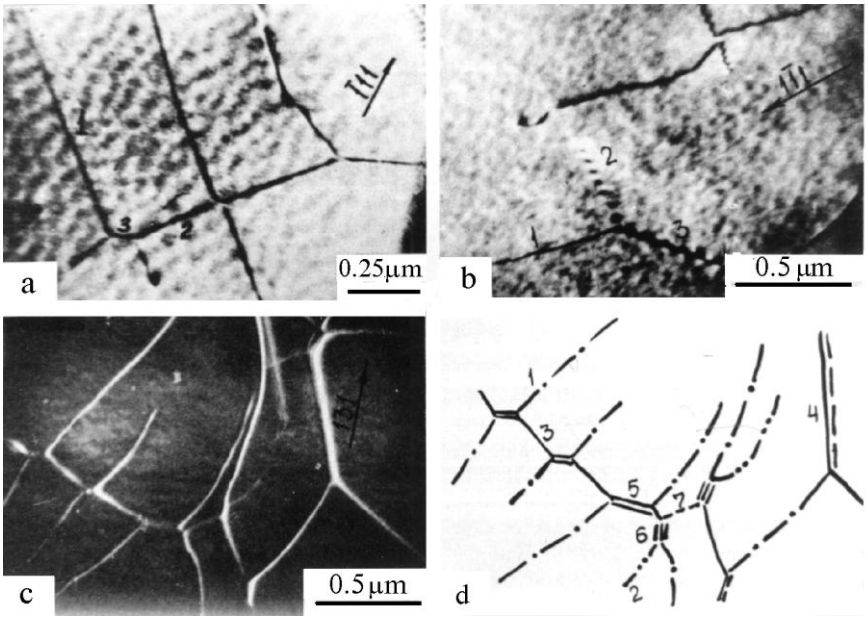

Figure 10. Microstructure of Ti–50Al after deformation at 800°C: a–c—dark-field images of node cascade recorded with **g** = [1 $\bar{1}$ 1]; (d) schematic picture. Dislocations with Burgers vector: 1—1/2[110], 2—1/2[1 $\bar{1}$ 0], 3—1/2[$\bar{1}$ 12], 4—[011], 5—[10 $\bar{1}$], 6—[010], 7—1/2[11 $\bar{2}$] (see [32]).

3.5. The Comparison of the Results for CuAu Ordered Alloy and TiAl

To gain a deeper insight into the nature of TiAl, the deformation behaviours of TiAl and CuAu alloys were compared. The anomaly of the yield stress was detected [37] for the polycrystal of ordered CuAu alloy without the lamellar structure.

It is known that the critical temperature T_c, for ordering of the CuAu alloy is 410°C and, besides, CuAuII is the equilibrium phase within the interval from 385°C to 410°C. The regimes of thermomechanical treatment were selected using appropriate TTT curves [38]. As a result a polycrystal of CuAuI had relatively coarse grains (5 to 10 μm) and was almost free of the lamellar structure. Mechanical tests were performed within the temperature interval from −196°C to 350°C. Foils for TEM analysis were prepared using a standard technique from sample deformed to 3%.

Figure 11 shows the yield stress $\sigma_{0.2}$ as a function of the test temperature. From Fig. 12 it is seen that $\sigma_{0.2}(T)$ exhibits a nonmonotonous temperature trend with a maximum near $T_{max} \cong 300$°C. The $\sigma_{0.2}$ value at T_{max} is nearly twice as high as the value at room temperature. A detailed

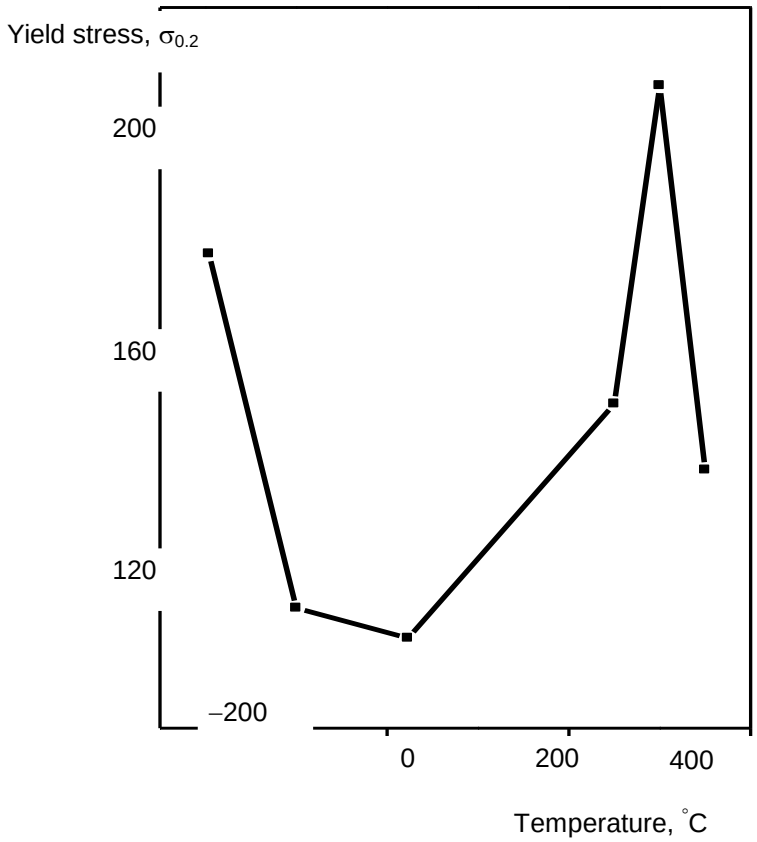

Figure 11. Temperature dependence of the yield stress $\sigma_{0.2}(T)$ of the CuAu ordered alloy [37].

analysis of the microstructure of the CuAu alloy deformed at various temperatures can be found elsewhere. Both single dislocations and superdislocations with the Burgers vectors ⟨101] and 1/2⟨112] were observed. Moreover, numerous microtwins were seen. APB bands in the cube plane were also detected. Figures 12 and 13 illustrate typical fragments of the microstructure of the CuAu alloy deformed at different temperatures.

Blocked ⟨101] superdislocations were observed in the region of the anomalous temperature trend. The long rectilinear dislocation in Fig. 13b was identified as a screw superdislocation. In addition, a characteristic configuration was observed: the so-called ‘tree’. The trunk had a fragmented structure, which included segments of superdislocations having both ⟨101] and 1/2⟨112] Burgers vectors. This configuration was observed in TiAl (Fig. 8). In CuAu, the configurations of the ‘tree’ type appeared even at room temperature (Fig. 13a) and persisted to the temperature T_{max}. Blocked dislocations were not detected among a host of

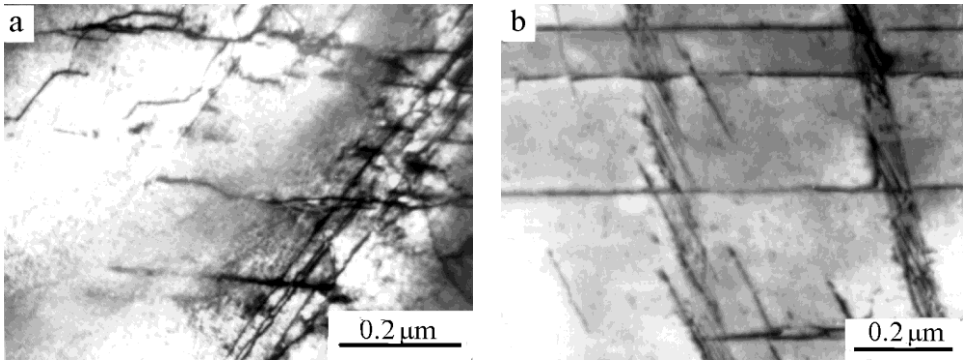

Figure 12. Microstructure of the CuAu ordered alloy deformed by 3% at −196°C, bright-field image of dislocations (courtesy O. V. Antonova and N. V. Kazantseva).

single dislocations clearly seen in Fig. 13. It was surprising to observe blocked dislocations at −196°C (Fig. 12). Their type has not been identified so far. Referring to the very fact of their observation, one can draw an analogy with observation of blocked dislocations in TiAl at −196°C (Fig. 7).

The nonmonotonous temperature dependence of $\sigma_{0.2}(T)$, which is obtained for the CuAu polycrystal (Fig. 11), is similar to the dependence observed for the TiAl single crystal (Fig. 1). For the sake of comparison the $\sigma_{0.2}(T)$ curve was obtained for the CuAu alloy with the grain size (~0.5 μm) much smaller than in the alloy under study. It was found that the nonmonotonous temperature trend is replaced by a plateau (~270 MPa). A similar dependence was observed for TiAl polycrystals with fine grains [39, 40]. It is worth noting that the mean grain size, at which the anomalous $\sigma_{0.2}(T)$ vanishes, is much smaller in CuAu than in TiAl.

In CuAu alloy, unlike in TiAl alloy, blocking of single dislocations was not detected in the region of the anomalous temperature behaviour of $\sigma_{0.2}(T)$. This fact is an evidence that in TiAl single dislocations are blocked through a special mechanism, which is related to features of the TiAl intermetallic itself rather than those of the $L1_0$ superstructure. The observation of the anomalous $\sigma_{0.2}(T)$ in CuAu is due to the fact that compatibility of deformation for a polycrystal always requires multiple slip.

4. ON THE POSSIBILITY OF CHANGES IN THE POTENTIAL RELIEF NEAR A MICROCRACK

If the yield stress has a nonmonotonic temperature dependence, the temperature dependence of plasticity $\delta(T)$ for TiAl includes low plasticity up to the temperature T_{max} of the $\sigma_y(T)$ peak, after which $\delta(T)$ increases with elevating temperature. A combination of a small yield stress and low plasticity at room temperature is unusual.

Room temperature is at the boundary between regions I and II. As stated earlier, a low σ_y value corresponds to g↔s transitions, *i.e*. capture of dislocations in shallow traps and their release from these traps. Deep traps do not show up themselves yet. The potential relief in region I actually acquires a shape similar to the one typical of b.c.c. metals (Fig. 3a). However, the shape of the potential relief can change in the vicinity of a microcrack. Indeed, it is known that a stress field alters the structure of a dislocation core. An example relating to a 1/2⟨112] superdislocation was considered in section 3.4.

Consider a configuration consisting of a crack and its associated screening dislocations. Assume that the characteristic crack stress–

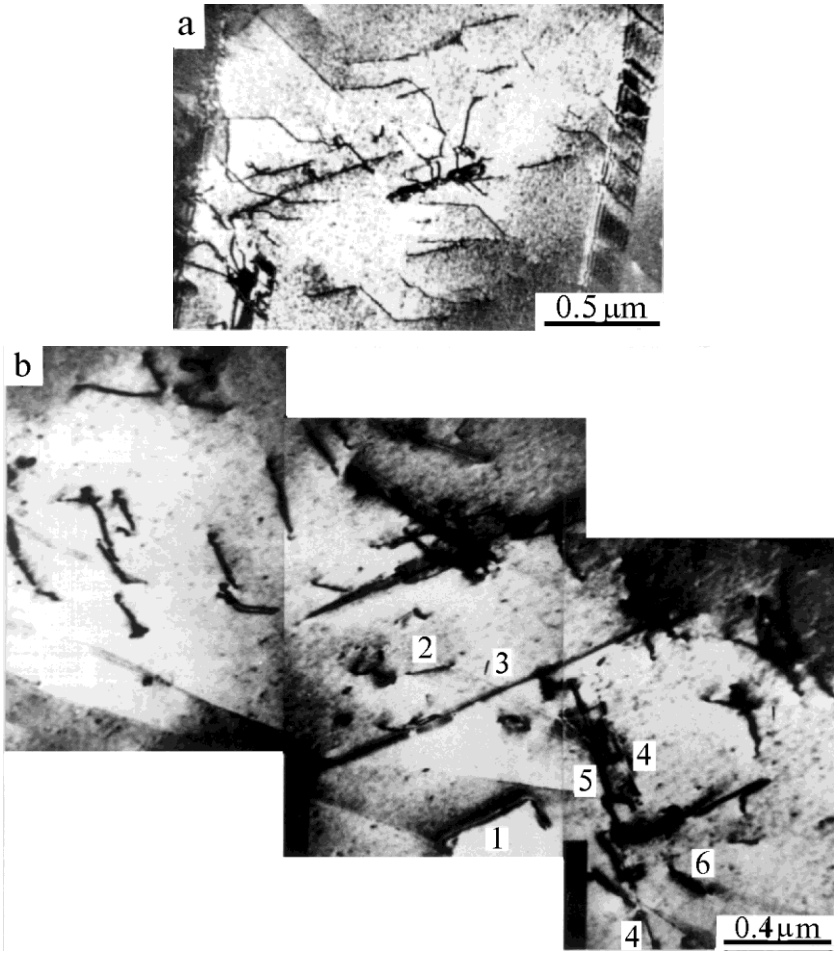

Figure 13. Microstructure of the CuAu ordered alloy deformed by 3%: a—at room temperature, dark-field image of dislocations in the reflection **g** = [020], BD = [10 $\bar{1}$]; b—at 250°C, bright-field image of dislocations [37].

concentration around the crack tip would shrink a wide core of the dislocation. Consequently, the dislocation would be captured in deep traps more easily. For a single dislocation this would mean that the dislocation drops more readily to deep Peierls valleys.

However, one and the same elastic field cannot simultaneously compress and expand a dislocation core. Therefore, if blocking of a single dislocation is facilitated near a crack, its release from a deep valley will not be easier than in the bulk of the material.

This assumption can be formulated as follows: the 'hill' separating g- and s′-states is truncated due to the stress concentration, but the potential well, which corresponds to the s′-state, remains deep. As a result, the potential relief approximates in shape the relief typical of semiconductors (Fig. 3b).

The presumed change of the potential relief near a microcrack should considerably affect operation of dislocation sources in this area. From analysis of shielding of a crack by a dislocation, it is conjectured that the ubiquitous presence of dislocation sources in metals assures generation of copious dislocations. The one dislocation with shielding Burgers vector will be repelled from the crack, and the other with antishielding Burgers vector will be attracted to the crack and cause a crack-opening displace-

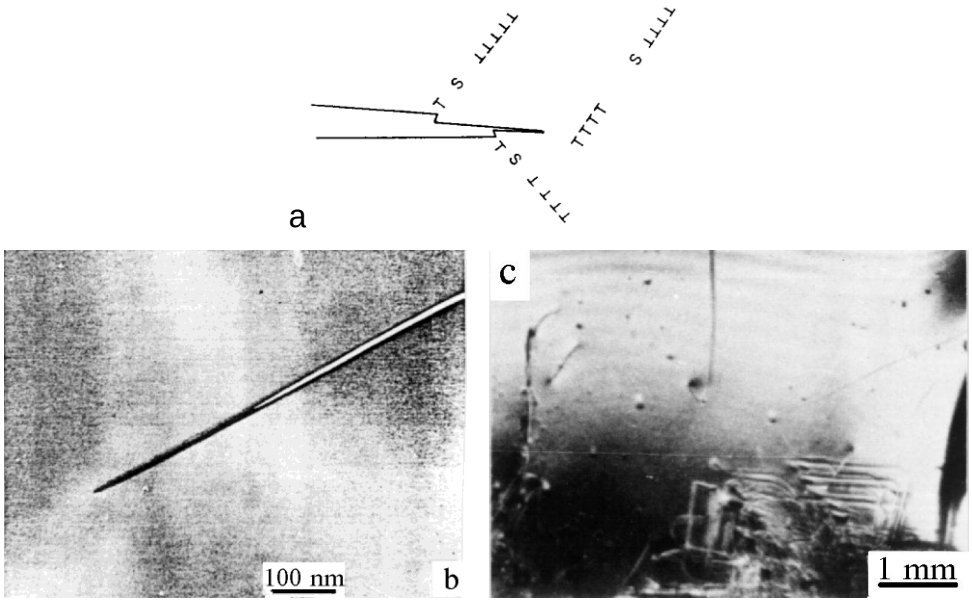

Figure 14. A crack and dislocations in plastic zone: a—dislocation sources (S) operate external to a crack and cause a crack-opening displacement [41]; b—a fully brittle crack in Si [41]; c—sessile configuration of 1/2<011> screw dislocations after nucleation of a crack in α-sulphur; a crack is located at bottom right of micrograph [42].

ment (Fig. 14a) [41].

Sharp cracks, near which dislocations are not seen, *i.e.* dislocation sources are inoperative, are observed in exceptional (non-metal) cases only. Such a crack in Si is shown in Fig. 14b. Taking into account similarity of the temperature dependences $\delta(T)$ observed for semiconductors [18] and TiAl, one can assume that a similar situation is realized in TiAl, despite different temperature dependences $\sigma_y(T)$ of these materials (see Fig. 2b, d).

Let us consider switch-on of dislocation sources in the bulk of the material and in the vicinity of a crack. A low σ_y value corresponds to easy switch-on of sources in the bulk at room temperature. However, the stress concentration near the crack facilitates g→s′ transitions and, thus, decreases the free path length λ_F. Consequently, the stress σ_F, which is required to switch on a dislocation source, 'automatically' increases in accordance with (8). Therefore, instead of facilitating an intensive operation of sources, as it usually does in materials with a low yield stress, the elastic field of the crack causes blocking of sources in TiAl. Moreover, if a dislocation from the bulk enters the plastic zone of a crack, it becomes blocked too. In this sense, the plastic zone of a crack itself acts as a large trap for dislocations and causes their blocking.

Up to now, blocking of single dislocations in deep Peierls valleys was considered as an example. However, low plasticity is also observed at orientations, which have not single dislocations. One may think that transformation of the wide core of a superpartial dislocation to the constricted form is rendered easier near a crack. Therefore, transformation of a ⟨101] superdislocation to a blocked Kear–Wilsdorf configuration or a nucleus of this configuration with a minimum width in the cube plane is facilitated. In either case, a band of a superstructural stacking fault appears. This impedes, as stated earlier, the reverse s′→g transformation of the ⟨101] superdislocation.

Di Persio and Escaig [42] obtained TEM data providing evidence that high stress near a crack favours the glissade–sessile transformation of a dislocation. Dislocations in the sessile form are clearly seen near a forthcoming crack in Fig. 14c. Although these results were obtained for α-sulphur and not for TiAl, they confirm that a crack field can induce blocking of dislocations.

Thus, a combination of a small yield stress and low plasticity, which is observed in TiAl at room temperature, is explained by two types of dislocation traps: shallow traps are responsible for small σ_y, while deep traps are the cause of low δ. As a result, TiAl has an unusual structure: the bulk of the material, where dislocation sources can be easily switched on, and inserts of the semiconductor type (plastic zones of cracks), where dislocation sources are blocked.

In our opinion, capture of dislocations in deep traps, which is stimulated by concentration of stresses near a crack, and stay of dislocations in these traps up to the temperature T_{max} lead to low plasticity in regions I

and II at any orientation of a single crystal. The fact that in TiAl $\delta(T)$ starts growing near T_{max}, when dislocations are unblocked intensively, confirms the supposition that brittleness of TiAl is connected with blocking of dislocation sources.

The comparison of $\delta(T)$ trends for TiAl and Ni_3Al [2] suggests that the barrier for the g→s′ transition in Ni_3Al is much higher than in TiAl. Therefore the decrease of the barrier near a microcrack in Ni_3Al is not so dramatic as in TiAl. Correspondingly, Ni_3Al alloy looses less in plasticity. Plasticity decreases only on approaching the temperature T_{max}. This fact also attests to a relationship between the ductile–brittle transition and blocking of dislocation sources.

Thus, an efficient method for improving plasticity of TiAl may be alloying with certain impurities that would favour growth of the potential barrier for the g→s′ transition of a dislocation to a deep trap.

5. ANALYSIS OF TRANSITION FROM THE HIGH-TEMPERATURE STEP TO THE LOW-TEMPERATURE STEP OF DEFORMATION

5.1. Reversibility and Irreversibility of $\sigma_y(T)$

One of schemes of two-step deformation is as follows: the first step includes small deformation (1–3%) at a high temperature T_1, which is however lower than the temperature T_{max} of the $\sigma_y(T)$ peak; the second step is realized at a temperature T_2, which normally is equal to room temperature.

Experiments performed by this scheme on alloys type Ni_3Al [43–45] showed that on transition from the high-temperature (HT) step to the low-temperature (LT) step the stress sharply decreased (stress macrojump) almost to the yield stress $\sigma_0(T_2)$ observed in the case of one-step LT deformation, which in what follows is taken as the reference value. Those results were treated as an evidence of reversibility of the yield stress, in line with the known experiments due to Cottrell–Stokes [46].

Some experiments [11] revealed a stress macrojump during two-step deformation of TiAl, as in the case of Ni_3Al, while in other experiments [47, 48] the stress achieved by the end of the HT step remained almost unchanged on transition to the LT step: no reversibility of $\sigma_y(T)$ was observed. Figure 15 shows $\sigma(\varepsilon)$ curves for two-step deformation of TiAl. A stress macrojump is observed at the orientation [$\bar{2}$ 51], while no stress macrojump occurs at the orientation [010].

A contradictory picture arises: On the one hand, an anomalous dependence $\sigma_y(T)$ should cause a drop of the stress with decreasing temperature. On the other hand, the stress should be preserved if the dislocation structure is not recovered on transition to the LT step.

A model [49] was proposed for description of two-step deformation. This model is based on an additive formula for the flow stress σ written as

$$\sigma = \sigma_F(T) + \sigma_{WH}(T, \varepsilon, \dot{\varepsilon}) \tag{22}$$

Here $\sigma_{WH}(T, \varepsilon, \dot{\varepsilon})$ is the stress increment caused by deformation strengthening ($\dot{\varepsilon}$ will henceforth be omitted since the deformation rate $\dot{\varepsilon} = \text{const}$ under dynamic loading). It is assumed that only $\sigma_{WH}(T, \varepsilon)$ depends on the dislocation density ρ. Then, in the case of two-step deformation the switch-on stress of a dislocation source $\sigma_F(T)$ changes reversibly on transition to the LT step and becomes $\sigma_F(T_2)$, which coincides with the reference yield stress $\sigma_0(T_2)$ measured without preliminary deformation. It is thought simultaneously that the quantity $\sigma_{WH}(T, \varepsilon)$ preserves its value $\sigma_{WH}(T_1)$ achieved by the end of the HT step, because density of

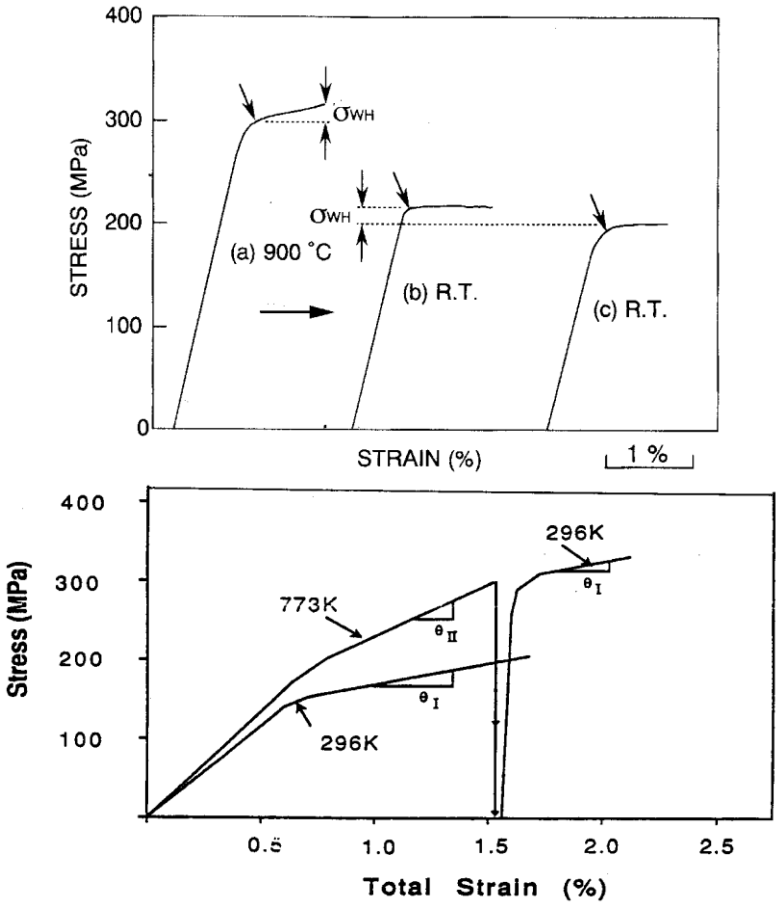

Figure 15. Two-step deformation of TiAl: a—thermal reversibility of flow stress for [$\bar{2}$ 51]-oriented crystal, in which ⟨101] superlattice slip is operative [11]; b—stress-strain curves for [010]-oriented crystal; lower curve, compression at room temperature; upper curves, two-step straining [47].

the blocked dislocation structure remains unchanged with decreasing temperature. Thus, in terms of the theoretical model in question, the plastic flow at the LT step starts at the stress

$$\sigma_y(T_2) = \sigma_0(T_2) + \sigma_{WH}(T_1). \tag{23}$$

From (23) it follows that the observed deviation from reversibility of $\sigma_y(T)$ (in other words, deviation of the yield stress at the LT step from the reference value) is determined by $\sigma_{WH}(T_1)$, which describes an increase in the stress at the expense of strengthening at the HT step. In some instances this deviation indeed is nearly equal to $\sigma_{WH}(T_1)$ (see, for example, Fig. 15a).

In a known experiment [43], however, the yield stress at the LT step differed little from the reference value, while $\sigma_{WH}(T_1)$ was high. When experimental data obtained for various orientations [45] were processed [50] by the said scheme using relation (23), the stress $\sigma_{WH}(T_1)$ proved to be too high or too low with respect to the observed deviation from reversibility of $\sigma_y(T)$.

Finally, the model [49] does not allow for possible conservation of the flow stress on transition to the LT step. Indeed, if (22) is true, the stress should drop nearly by $\{\sigma_0(T_1) - \sigma_0(T_2)\}$ on transition from the HT step to the LT one. But no macrojump was observed in the aforementioned experiments [47, 48].

5.2. Transparency of the Dislocation Framework and Stress Macrojump

Since interpretation of experimental results in terms of the model [49] encounters certain difficulties, we have proposed an alternative approach [26, 51, 52] and abandoned the additive formula (22) for the flow stress.

Earlier we introduced two threshold stresses (3) and (10), which determine the onset of plastic flow in different cases. In a general case, in the presence of a dislocation structure formed beforehand, the condition of plastic flow should act as a ‘double key’, which ensures both operation of sources and the possibility to overcome the elastic counteraction of the dislocation structure. This condition can be written in the form:

$$\sigma_y(T) = \max\left\{\sigma_F(T), \kappa\sqrt{\rho}\right\}. \tag{24}$$

Validity of expression (24) was convincingly proved by Ezz and Hirsch [49] who obtained the temperature dependence of the yield stress $\sigma_{yp}(T)$ for $Ni_3(Al,Hf)B$ intermetallic, which was subject to a strong cold deformation beforehand. Figure 16 shows schematically $\sigma_{yp}(T)$ plotted [49] using a set of experimental data.

The trend of the yield stress in the absence of cold deformation is

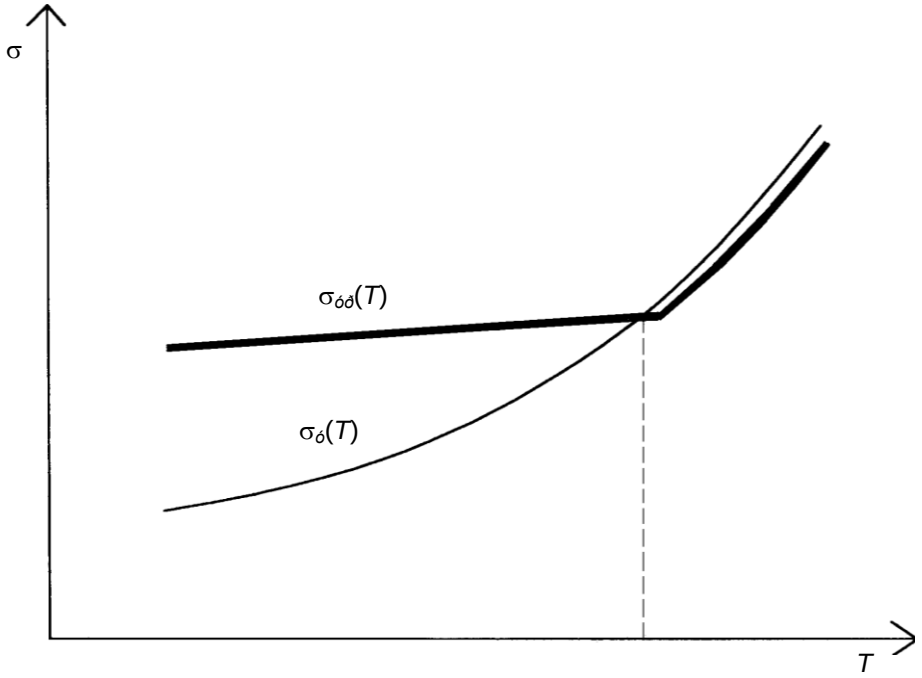

Figure 16. Schematic of yield stress temperature dependence for $Ni_3(Al,Hf)B$ after preliminary cold deformation [49].

shown for comparison. The curve $\sigma_{yp}(T)$ has a plateau, which testifies to conservation of the stress caused by preliminary deformation. In other words, the aforementioned reversibility does not take place in the temperature interval of the plateau. Subsequently the plateau changes to an anomalous temperature trend at a certain temperature. So, the observed curve $\sigma_{yp}(T)$ indeed has a shape, which can be described by expression (24) and cannot be described by expression (23).

Using (24), we made an effort to construct a model of deformation behaviour of the intermetallic that would combine two seemingly incompatible options: observation or absence of a macrojump.

Let us first consider superdislocations $\langle 101 \rangle$. This is the only type of dislocations in Ni_3Al, but TiAl can contain other types of dislocations as will be discussed below. During the HT step, when $T_1 < T_{max}$, a microstructure with a high density of dislocations ρ_1 appears. Since superdislocations are blocked, this microstructure represents a rigid framework comprising Kear–Wilsdorf barriers. These barriers are indestructible in the interval of an anomalous trend of $\sigma_y(T)$ and therefore they can hardly transform to glissade dislocations on transition to the LT step of deformation. Consequently, the framework is inherited in the absence of recovery and a high density of dislocations is preserved at the LT step. In accor-

dance with (3), the stress achieved by the end of the HT step is

$$\sigma_1(T_1) = \kappa\sqrt{\rho_1} > \sigma_F(T_1). \tag{25}$$

If the same slip system(s) continues operating at the LT step, plastic flow at a low temperature T_2 of the second step should start at a stress

$$\sigma_2(T_2) \approx \max\left\{\sigma_F(T_2), \kappa\sqrt{\rho_1}\right\}. \tag{26}$$

Since the stress $\sigma_F(T)$ exhibits an anomalous trend, then

$$\sigma_F(T) < \sigma_F(T_1) < \sigma_1(T_1). \tag{27}$$

Consequently, at first glance, the following equality should be fulfilled:

$$\sigma_2(T_2) \cong \kappa\sqrt{\rho_1} \cong \sigma_1(T_1). \tag{28}$$

Therefore the stress cannot drop lower than $\sigma_1(T_1)$ with decreasing temperature.

In our opinion, the situation can change if a new slip system operates at the LT step. In this case the framework inherited from the HT step does not contain dislocations of the new slip system. Let us simplify the task and assume that only one slip system I with the Burgers vector $\mathbf{b_I}$ operates at the HT step. The key question is: can the dislocation framework turn transparent on transition to the LT step and, simultaneously, preserve its structure and density? Let the Burgers vector $\mathbf{b_{II}}$ for a new slip system II be perpendicular to $\mathbf{b_I}$ so that vectors $\mathbf{b_I}$ and $\mathbf{b_{II}}$ are parallel to diagonals of one and the same cube face. In this case, any of possible slip planes {111} is parallel to one of these vectors (Fig. 17).

As a result, the framework axes do not lie in possible slip planes II but cross them. The framework acts as a 'forest' with respect to dislocations of the slip system II. Without going into detail of local interaction between nonparallel dislocations we shall note only that in this case the dependence of the type of $1/r$ on the distance r between dislocations, which is characteristic of the force of elastic interaction between parallel dislocations, vanishes [53]. But it is this dependence that underlies the relation (3).

Taking into account the framework rigidity and mutual perpendicularity of vectors $\mathbf{b_I}$ and $\mathbf{b_{II}}$, one may expect the elastic counteraction of the framework to dislocations II to be weak. Since the system II is devoid of its own framework, from (24) we readily have

$$\sigma_2(T_2) \approx \sigma_F(T_2) < \sigma_1(T_1). \tag{29}$$

So, it is with this assumption that a macrojump of the stress can be observed on transition to the LT step of deformation.

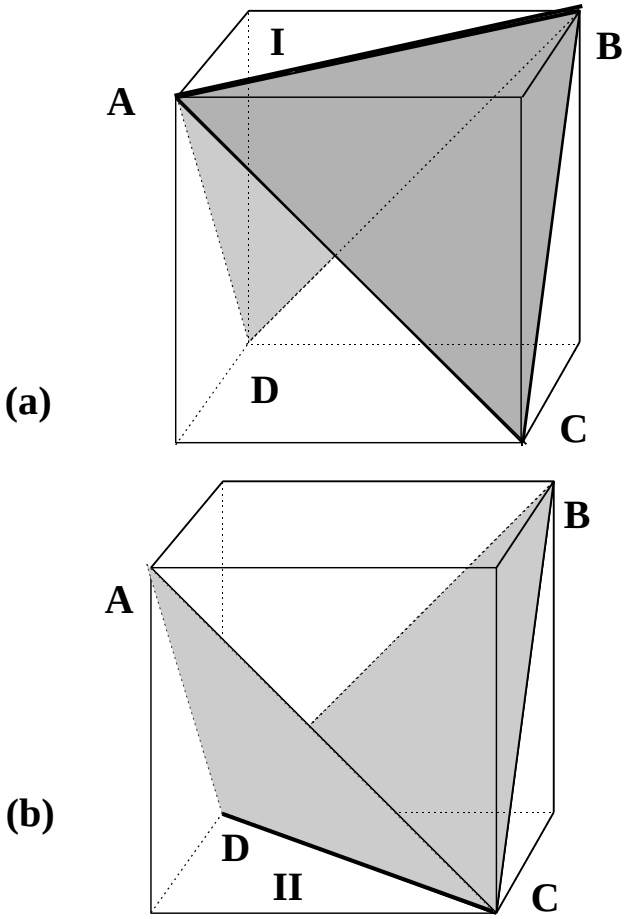

Figure 17. Slip planes {111} whose intersection lines are parallel to different diagonals of one and the same cube face.

Two points, which are significant on transition from the HT to the LT step, can be emphasized. Firstly, it is an anomalous trend of the yield stress and, correspondingly, a drop of the stress $\sigma_F(T)$ with decreasing temperature. Secondly, a slip system II, whose dislocations experience little elastic counteraction from the framework, can come into play.

This brings about a question why system II is not involved at the first step even if, as it often happens in prestraining experiments, Schmid factors of systems I and II are nearly equal.

5.3. Mechanism Initiating Blocking of a Dislocation Source

Taking into account what has been said above, it is reasonable to think of

a mechanism that would prevent the switch-on of system II at the HT step and allow its switch-on at the LT step. Also, this mechanism should not hinder the switch-on of slip systems where Burgers vectors are parallel to different cube faces. Such slip systems indeed were observed at the HT step [43] and also during one-step deformation in the interval of an anomalous trend of $\sigma_y(T)$ (see, for example, [54]).

So, the mechanism in question should be connected with thermally activated blocking, which takes place in one cube face whose diagonals are vectors $\mathbf{b}_{\mathrm{I}}$ and $\mathbf{b}_{\mathrm{II}}$. Transformation of a glissade superdislocation to a Kear–Wilsdorf barrier may be thought of as thermally activated blocking. Obviously, such barriers are formed through slip to one and the same cube face for systems I and II only. It is this circumstance that distinguishes systems I and II among the whole set of octahedral slip system.

Let us consider collision of a glissade superdislocation II and a blocked superdislocation I. Consecutive blocking stages of a superdislocation II are shown in Fig. 18.

This process includes formation of a constriction in the superpartial dislocation, recombination and bending of the recombined segment in the cube plane [55, 56]. Barrier I stimulates the cross-slip of a screw superdislocation II to the cube plane, because part of the APB band, which belongs to barrier I, disappears in the cube plane. For this reason, the activation energy for a superpartial dislocation II to slip under the action of barrier I to the cube plane is nearly equal to the recombination energy of this dislocation. The latter energy is lower than the activation energy of barrier I formation. This is also true for the cross-slip through generation and propagation of kinks.

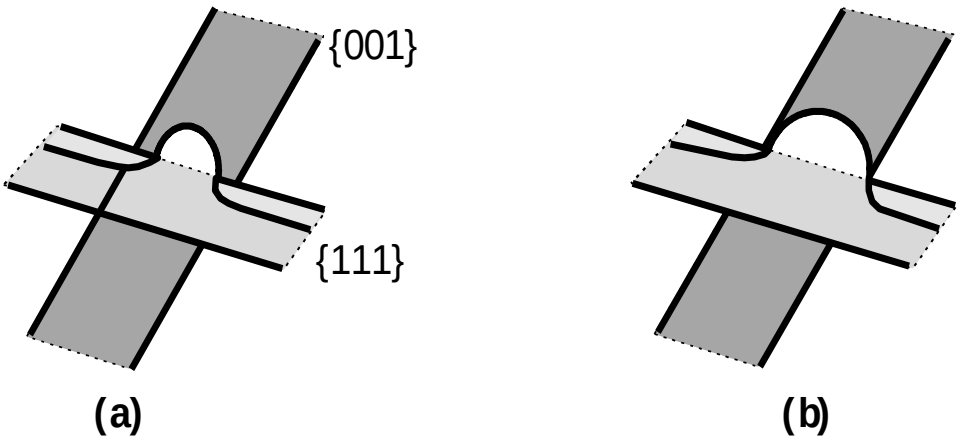

Figure 18. Cross-slip of superpartial dislocation followed by vanishing of the APB band in the cube plane; (a) and (b)—different stages of recombined segment bending [55].

Assume that the slip system I is switched on first at the HT step and produces a framework with a high density of dislocations. Superdislocations II, which have already been present in the initial state, are stopped by this framework (Fig. 18a). Segments of a superdislocation II, which are located between 'forest trees', represent potential dislocation sources. However, each 'tree' includes the aforementioned APB band. A blocked configuration II nucleates (see Fig. 18b). Blocking may develop along the superdislocation. Clearly, only a screw segment is blocked. However, if the framework stops an edge superdislocation II, a screw segment, which appears upon bending of this superdislocation, also extends along the aforementioned APB band and slips to the cube plane. Thus, potential sources represented by superdislocations II and stopped by the framework are blocked. The mechanism of contact interaction, which we have just discussed, represents the mechanism in question responsible for blocking of sources of dislocations having similar Schmid factors. If one of the systems is switched on first, the said mechanism suppresses the switch-on of the other system. This applies only to slip systems with mutually perpendicular Burgers vectors. As follows from the above discussion, 'the second diagonal inhibit' is ineffective with respect to diagonals of different faces.

It remains to clarify why systems I and II cannot be switched on simultaneously at the HT step. This fact may be attributed to a deviation from precise orientation. Even a slight deviation is sufficient for Schmid factors to be dissimilar. If it is assumed that dislocations multiply in an avalanche manner, one system immediately leads the other. Later, sources of the system II cannot be switched on at the HT step because of mechanism initiating the blocking. However, they can be switched on at the LT step if recombination of a superpartial dislocation is impeded and the said mechanism does not operate.

5.4. Comparison of Two-Step Deformation of TiAl and Ni_3Al

Maximum Schmid factors for possible types of dislocations are given in Table 1 for orientations at which TiAl underwent two-step deformation (references are given in the heading).

A stress macrojump was detected in TiAl only at the orientation $[\bar{2}\,51]$ among all orientations studied (see Fig. 15a). A similar orientation, namely $[\bar{1}\,25]$, was examined in $Ni_3(Al,Ti)$ where a stress macrojump was revealed too [45]. From Table it is seen that the Schmid factor is a maximum at the orientation $[\bar{2}\,51]$ of the superdislocation $\langle 101]$ among all other types of dislocations possible in TiAl. Only one superdislocation slip system with the Burgers vector [011] has the Schmid factor equal to 0.490. The superdislocation slip system with the perpendicular Burgers vector $[0\,\bar{1}\,1]$ has a smaller Schmid factor equal to 0.435. Only the first slip system is observed at the HT step [11]. Other types of dislocations

TABLE 1. Maximum Schmid factors for possible types of dislocations.

	[11]	[47]	[48]	[48]
	$[\bar{2}\,51]$	[010]	[011]	[001]
1/2⟨110]	0.381	0.405	0.405	0
⟨101]	0.490	0.405	0.405	0.405
1/2⟨112]	0.424	0.230	0.230	0.470

were not observed at this orientation.

Considering the model proposed above, we suppose that the stress macrojump is due to the switch-on of a slip system II with the Burgers vector $[0\,\bar{1}\,1]$ at the LT step. Taking into account that slip systems I and II have the Schmid factor ratio of ~ 1.14 and considering the data in Fig. 15a, we immediately have that the resolved stress for the system II, which corresponds to the beginning of the LT step, almost coincides with the reference stress, *i.e*. the resolved stress for the system I in the case of one-step LT deformation.

Slip systems of single dislocations can operate at orientations [010] and [011], at which no stress macrojump was observed in TiAl [47, 48]. From Table it is seen that their maximum Schmid factors ($f = 0.405$) coincide with the corresponding factors of superdislocation systems. Consequently, in addition to superdislocation slip systems, two slip systems of single dislocations corresponding to diagonals of the (001) face can be switched on at the HT step. Note that they have equal Schmid factors at the given orientations. The 'second diagonal inhibit' does not apply to these single dislocations, because their blocking is not associated with formation of Kear–Wilsdorf barriers. Both slip systems of single dislocations with mutually perpendicular Burgers vectors were actually observed in [32] (see Fig. 9c) and also in [11]. In this case, as can be seen from Fig. 17, any of possible octahedral slip planes includes blocked dislocations of the framework. Consequently, the framework cannot turn transparent to any new slip system on transition to the LT step.

No stress macrojump is observed either at the orientation [001], although single dislocations are absent. However, superdislocations with three possible Burgers vectors type 1/2⟨112] have a maximum Schmid factor. It is not improbable that these slip systems can be switched on. In this case the framework structure will be more complicated than the one considered above. Such framework can hardly turn transparent on transition to the LT step.

A feature in common of orientations [010] and [001], which are not

equivalent in TiAl, is that slip systems of single dislocations or superdislocations 1/2⟨112] can be switched on in addition to slip systems of superdislocations ⟨101]. Different types of dislocations present in TiAl complicate the framework structure and make the picture of transition from the HT to the LT step smeared. A stress macrojump is always observed in ⟨001⟩ single crystals of Ni_3Al, unlike in TiAl, during two-step deformation [43, 45]. These two intermetallics need be analysed at same orientations to determine causes responsible for their different or similar behaviour during two-step deformation.

6. CONCLUSION

This review offers a wider concept of the multivalley Peierls relief in TiAl. An earlier model [20] included a blocking mechanism of single dislocations by their immersion in deep Peierls valleys. That mechanism explained observation of single dislocations in glissade and sessile forms. But it failed to describe the whole curve $\sigma_y(T)$. Using TEM data on evolution of the dislocation structure and comparing deformation curves for TiAl with typical curves for other materials, we made an effort to reconstruct the shape of the potential relief for a dislocation in TiAl. In our opinion, a complicated potential relief, which is schematically shown in Fig. 3d, corresponds to the deformation behaviour of TiAl. This relief includes (i) potential wells of different depth corresponding to two types (shallow and deep) traps, and (ii) potential barriers of different height: low and high barriers for capture of dislocations in shallow and deep traps respectively. These representations were used to describe a nonmonotonic temperature dependence of the yield stress. It was conjectured that the shape of the potential relief for a dislocation changes in the plastic zone of a microcrack.

The supposition on the presence of two types of dislocation traps is confirmed, firstly, by the fact that the yield stress drops first in the low-temperature interval and then in the high-temperature interval, and, secondly, by observation of blocked dislocations both at extremely low temperatures and in the region of an anomalous trend of $\sigma_y(T)$. One may think that pulsation of the wide core of a dislocation, which is due to thermal fluctuations, leads to local narrowing of the core. Such random changes of the core structure are fixed thanks to the capture of a recombined segment in deep valleys in the case of a single dislocation or cross-slip to the cube plane in the case of a superpartial dislocation. Ultimately, a dislocation is captured in a deep trap.

Numerous unusual features of the deformation behaviour of TiAl, which apparently are independent of one another, actually stem from a single effect. This effect is thermally activated blocking of dislocation sources. It is the temperature dependence of the dislocation source switch-on stress $\sigma_F(T)$ that determines a temperature anomaly of $\sigma_y(T)$.

The fact that the stress σ_F is independent of the strain rate explains a weak strain-rate sensitivity of the flow stress observed in the interval of the anomalous trend. All other factor being equal, a system with a lowest σ_F operates out of other slip systems. This consideration can account for disappearance of certain types of dislocations in certain temperature intervals. Concentration of stresses causes blocking of dislocation sources near a microcrack, possibly leading to TiAl embrittlement. The stress σ_F fits naturally the condition (26), which determines the onset of plastic flow in description of prestraining experiments. We assume that when a stress macrojump is observed, the low-temperature step begins at the switch-on stress of a new slip system, for which a dislocation framework inherited from HT step is transparent.

ACKNOWLEDGEMENTS

The authors would like to thank INTAS-97-31994 and the Russian Fundamental Research Foundation (Grant No. 98-02-17278) for financial support.

REFERENCES

1. D. P. Pope and S. S. Ezz, *Int. Metall. Rev.*, **29:** 136 (1984).
2. T. Suzuki, Y. Mishima, and S. Miura, *ISIJ International*, **29:** 1 (1989).
3. H. A. Lipsitt, D. Schechtman, and R. E. Schafric, *Metall. Trans. A*, **6:** 1991 (1975).
4. D. M. Dimiduk, *Gamma Titanium Aluminides* (Eds. Y.-W. Kim et al.) (Warrendale, PA, USA: TMS: 1995), p. 3.
5. Y. Umakoshi, H. J. Yasuda, and T. Nakano, *Intermetallics*, **4** Supplement: p. S65 (1996).
6. D. Banerjee, A. K. Gogia, T. K. Nandi, and V. A. Joshi, *Acta Met.*, **36:** 871 (1988).
7. D. Banerjee, *Phil. Mag. A*, **72:** 1559 (1995).
8. P. K. Sagar, D. Banerjee, K. Muraleedharan, and Y. U. R. K. Prasad, *Met. Trans*. *A*, **27:** 2593 (1996).
9. T. Kawabata, T. Kanai, and O. Izumi, *Acta Met*., **33:** 1355 (1985).
10. T. Kawabata, T. Abumiya, T. Kanai, and O. Izumi, *Acta Met*. *Mater.*, **38:** 1381 (1990).
11. H. Inui, M. Matsumuro, D.-H. Wu, and M. Yamaguchi, *Phil. Mag*. *A*, **75:** 395 (1997).
12. B. A. Greenberg and M. A. Ivanov, *Mat. Sci. Eng*. *A*, **153:** 356 (1992).
13. M. A. Ivanov, B. A. Greenberg, and T. O. Barabash, *Phys. Met. Metallogr*., **86:** 240 (1998).
14. M. A. Ivanov, B. A. Greenberg, and N. A. Kruglikov*, Gamma Titanium Aluminides* (Eds. Y.-W. Kim et al.) (Warrendale, PA, USA: TMS: 1999), p. 256.
15. M. A. Ivanov, B. A. Greenberg, and N. A. Kruglikov, *Phys. Met. Metallogr*., **89:** in press (2000).
16. V. I. Trefilov, Yu. V. Mil'man, and S. A. Firstov, *Physics of Refractory-Metals' Strength* (Kiev: Naukova Dumka: 1975) (in Russian).

17. V. Vitek and M. Yamaguchi, *Interatomic Potentials and Crystalline Defects* (Ed. J. K. Lee) (Warrendale, PA, USA: TMS-AIME Publ: 1981), p. 223.
18. H. Alexander, *Dislocations in Solids* (Ed. F. R. N. Nabarro) (Amsterdam: Elsevier Sci. Publ: 1986), Vol. **7**, p. 113.
19. P. Veyssiere, *ISIJ International*, **31:** 1028 (1991).
20. B. A. Greenberg, V. I. Anisimov, Yu. N. Gornostirev, and G. G. Taluts, *Scripta metall*., **22:** 859 (1988).
21. S. Rao, C. Woodward, J. Simmons, and D. M. Dimiduk, *High Temperature Ordered Intermetallic Alloys VI: MRS Symp. Proc.* (1995), Vol. **364**, p. 129.
22. G. Hug, A. Loiseau, and A. Lasalmonie, *Phil. Mag*. *A*, **54:** 47 (1986).
23. D. M. Wee, D. P. Pope, and V. Vitek, *Acta metall*., **32:** 829 (1984).
24. B. A Greenberg and M. A. Ivanov, *Gamma Titanium Aluminides* (Eds. Y.-W. Kim et al.) (Warrendale, PA, USA: TMS: 1995), p. 299.
25. B. A Greenberg and M. A. Ivanov, *Met. Phys. Adv. Tech*., **16:** 1159 (1997).
26. B. A Greenberg and M. A. Ivanov, *Mat. Sci. Eng*. *A*, **239:** 813 (199**7)**.
27. B. A Greenberg and M. A. Ivanov, *Phys. Met. Metallogr*., **78:** 247 (1994).
28. G. Hug, A. Loiseau, and P. Veyssiere, *Phil. Mag*. *A*, **57:** 499 (1988).
29. G. Hug, A. Loiseau, and P. Veyssiere, *Revue Phys. Appl*., **23:** 673 (1988).
30. S. A. Court, V. K. Vasudevan, and H. L. Fraser, *Phil. Mag*. *A*, **61:** 14 (1990).
31. B. A. Greenberg, O. V. Antonova, V. N. Indenbaum, L. E. Karkina, A. B. Notkin, M. V. Ponomarev, and L. V. Smirnov, *Acta Metall. Mater*., **39:** 233; ibid., 243 (1991).
32. B. A. Greenberg, O. V. Antonova, L. E. Karkina, A. B. Notkin, and M. V. Ponomarev, *Acta Metall. Mater*., **40:** 815; ibid., 823 (1992).
33. M. A. Morris, *Phil. Mag*. *A*, **68:** 237; ibid., 259 (1993).
34. M. A. Morris, *Phil. Mag*. *A*, **69:** 129 (1994).
35. B. Viguier, K. J. Hemker, J. Bonneville, F. Louchet, and J. L. Martin, *Phil. Mag*. *A*, **71:** 1295 (1995).
36. S. Sriram, D. M. Dimiduk, P. M. Hazzledine, and V. K. Vasudevan, *Phil. Mag*. *A*, **76:** 965 (1997).
37. B. A. Greenberg, O. V. Antonova, and A. Yu. Volkov, *Intermetallics*, **7:** 1219 (1999).
38. B. A. Greenberg, G. Hug, O. V. Antonova, T. S. Boyarshinova, Z. M. Pesina, I. N. Sachanskaya, and A. Yu. Volkov, *Intermetallics*, **5:** 297 (1997).
39. V. K. Vasudevan, S. A. Court, P. Kurath, and H. L. Fraser, *Scripta Met*., **23:** 467 (1989).
40. S.-C. Huang and E. L. Hall, *Metall. Trans. A*, **22:** 427 (1991).
41. R.M. Thomson, *Phys. Metallurgy* (Eds. R.W. Cahn and P. Haasen) (Elsevier Sci. Publ. BV: 1983), p. 1487.
42. J. Di Persio and B. Escaig, *Dislocations 1984* (Eds. P. Veyssiere et al.) (Paris, France: CNRS: 1984), p. 267.
43. M. Dimiduk and T.A. Parthasarathy, *Phil. Mag. Lett*., **71:** 21 (1995).
44. X. Shi, G. Saada, and P. Veyssiere, *Phil. Mag*. *A*, **73:** 1419 (1996).
45. N. D. Bakhteyeva, B. A. Greenberg, A. V. Nemchenko, and Yu. N. Akshentsev, *Phys. Met. Metallogr*., **85:** 481 (1998).
46. S. J. Basinski and Z. S. Basinski, *Dislocations in Solids*: *IV Dislocations in Metallurgy* (Ed. F. R. N. Nabarro) (Amsterdam, North-Holland: 1979), Vol. **4**, p. 261.
47. M. A. Stucke, D. M. Dimiduk, and P. M. Hazzledine, *High Temperature Ordered Intermetallic Alloys V: MRS Symp. Proc.* (1993), Vol. **228**, p. 471.
48. R. Mahapatra, Y. T. Chou, and D. P. Pope, *Mat. Sci. Eng. A*, **239:** 456 (1997).

49. S. Ezz and P. B. Hirsch, *Phil. Mag*. *A*, **73:** 1969 (1996).
50. N. D. Bakhteyeva, B. A. Greenberg, A. V. Nemchenko, Yu. N. Akshentsev, M. A. Ivanov, and Eu. N. Khlystov, *Izvestiya Akad. Sci*., **63:** 42 (1999).
51. B. A. Greenberg, M. A. Ivanov, T. O. Barabash, and A. G. Blokhin, *Phys. Met. Metallogr*., **81:** 374; ibid., 381 (1996).
52. B. A. Greenberg and M. A. Ivanov, *Met. Phys. Adv. Tech*., **17:** 973 (1999).
53. B. A. Greenberg and M. A. Ivanov, *Phys. Met. Metallogr*., **79:** 1373 (1995).
54. A. E. Staton-Bevan and R. D. Rawlings, *Phys. status solidi (a)*, **29:** 613 (1975).
55. B. A. Greenberg and M. A. Ivanov, *Metallofiz. Noveishie Tekhnol*., **21**, No. 7: 55 (1999).
56. B. A. Greenberg and M. A. Ivanov, *Metallofiz. Noveishie Tekhnol*., **21**, No. 8: 3 (1999).